Tectonophysics xxx (2013) xxx–xxx

Contents lists available at SciVerse ScienceDirect

Tectonophysics

journal homepage: www.elsevier.com/locate/tecto

Geological control of the partitioning between seismic and aseismic sliding behaviours in active faults: Evidence from the Western Alps, France

J.-P. Gratier [a,*], F. Thouvenot [a], L. Jenatton [a], A. Tourette [a], M.-L. Doan [a], F. Renard [a,b]

[a] ISTerre, Université de Grenoble 1, CNRS, BP 53, Grenoble F-38041, France
[b] Physics of Geological Processes, University of Oslo, 0316 Oslo, Norway

ARTICLE INFO

Article history:
Received 25 June 2012
Received in revised form 31 January 2013
Accepted 4 February 2013
Available online xxxx

Keywords:
Creep
Fault
Pressure-solution
Seismic
Aseismic
Alps

ABSTRACT

Given that active faults can slide either continuously by aseismic creep or episodically during earthquakes, and that the same fault zone may evolve laterally from seismic to aseismic deformation, an important issue is to know whether seismic to aseismic transition can be geologically controlled. This article presents examples of contrasted mechanical behaviour along active faults that cross cut limestone and marl units within the sedimentary cover of the French Alps. By matching seismic events along strike-slip and normal faults with the nature and structure of the rocks, it is demonstrated that the partition between seismic and aseismic sliding at depth is geologically controlled: earthquakes nucleate in the strongest rocks, mainly limestones, whereas marls accommodate at least part of the tectonic loading by aseismic creep. By looking at exhumed rocks deformed in the same context it is possible to identify the mechanism of creep, which is shown to be pressure solution creep either as a permanent or post-seismic creep. As earthquakes slip are seen to propagate through the whole upper crust, creep processes do not necessarily prevent an earthquake rupture from propagating through creeping units. However, creep relaxes stress and consequently reduces the available elastic potential energy at the origin of earthquakes in such creeping zones. The key parameters of pressure solution creep laws are presented and discussed. Using these laws, it is possible to infer why marl may creep more easily than limestone or why highly fractured limestone may creep more easily than intact rock. This approach also identifies other rocks that could creep by pressure solution in subduction zones and indicates how creeping zones may act as barriers for earthquake rupture propagation. Finally, the criteria possibly revealing geological control of the transition between seismic and aseismic sliding at depth are discussed with respect to subduction zones.

1. Introduction

The mechanical behaviour of active fault zones involves a variety of sliding modes, from continuous aseismic creep to sudden rupture during earthquakes. Such contrasting behaviour may be observed in various contexts, such as subduction zones where seismic patches are surrounded by aseismic deformation zones (Masson et al., 2005; Satyabala et al., 2012), collision zones (Masson et al., 2005; Satyabala et al., 2012), and strike-slip faults (Evans et al., 2012; Nadeau et al., 2004). Even in the so-called "seismic zone", afterslip creep may accommodate part of the displacement (Freed, 2007). Consequently, aseismic creep, which occurs either as a continuous process or as post-seismic afterslip deformation, could significantly relax tectonic stresses and therefore reduce the occurrence of major earthquakes in these zones. A major issue is to understand whether the transition between seismic and aseismic behaviours could be controlled by the geological characteristics of the deformed rocks: are some types of rocks more prone to seismic failure while others are more prone to aseismic creep? To answer such a question, it is necessary to identify the grain-scale mechanisms of aseismic creep and then to investigate how such mechanisms may be sensitive to the nature, structure or composition of the rocks. Finally, if such geological control does indeed govern the transition between seismic and aseismic slips, how can the key geological characteristics controlling the seismic to aseismic transitions be recognized at depth?

To answer these questions, several examples are presented of contrasted rock behaviours along active faults that cross cut layers of limestones and marls within the sedimentary cover of the French Alps. This area of moderate seismicity has been carefully monitored over the past thirty years through a network of short-period seismometers, providing accurate locations of small seismic events. In a first step, the seismicity distribution along active strike-slip and normal faults (Vuache and Clansayes faults) was matched with the nature, structure and composition of the rocks that can be seen on the geological cross-section. These data indicate a lithological control of the transition between seismic and aseismic slips at depth because most earthquakes nucleate in the strong limestone units and only few of them could be observed in the weak marl units. However, in

* Corresponding author. Tel.: +33 685051784.
E-mail address: Jean-Pierre.Gratier@ujf-grenoble.fr (J.-P. Gratier).

0040-1951/$ – see front matter © 2013 Elsevier B.V. All rights reserved.
http://dx.doi.org/10.1016/j.tecto.2013.02.013

most cases, it is not possible to observe directly the rocks at depth, and therefore to identify the creep mechanisms. A second step therefore had to be introduced to provide additional constraints based on the Cléry fault zone that formed in the same geological context as the Vuache and Clansayes faults, and which was recently exhumed.

Stratigraphically analogous limestone and marl units, outcropping at the surface near the same type of recent Alpine exhumed faults, were studied in order to establish the mechanisms of the creep processes associated with seismic and aseismic deformations: either as permanent or post-seismic creep. Various mechanisms of creep in crustal rocks could be at work: i) pressure solution creep (Rutter, 1976) involves coupling fluid–rock interactions with deformation; ii) brittle creep (Chester et al., 2007; Heap et al., 2009) involves the generation and slow propagation of microcracks that weaken the rocks, iii) frictional processes such as low-friction deformation with talc-bearing phyllonite for example (Smith et al., 2012), or the presence of weak phyllosilicates such as saponite (Lockner et al., 2011), or the effect of fault fabric as well-developed foliation (Collettini et al., 2009). Frictional-viscous creep involves the coupling between pressure solution and frictional sliding (Bos and Spiers, 2002; Bos et al., 2000). "Mixed mode" deformation, with fault creep in a foliated phyllosilicate-rich fault zone and a seismic event initiating in more rigid competent lenses as dolomite or mafic blocks, has been described for example by Collettini et al. (2011), Faulkner et al. (2003).

The main result of the present work is that both long-term seismological monitoring, with high-resolution locations of earthquake foci at depth, and outcrop observations provide evidence that earthquakes rupture nucleate and propagate in the strongest rocks, mainly limestone, whereas marl units accommodate tectonic loading, mainly by aseismic pressure solution creep. This clearly reflects lithological control of the seismic to aseismic transition. However, creeping in a given type of rock does not necessarily prevent earthquake rupture from propagating through it, either because the creeping process does not completely relax the stress or as a result of dynamic processes of seismic interactions from neighbouring earthquakes. Moreover, the so-called seismic zones may also show afterslip creep. For both permanent and transient creep processes, the stress is relaxed, which therefore lowers the probability of occurrence of a new earthquake in these zones. Finally, since the creep mechanism has been identified in this work as pressure solution creep, the manner in which this mechanism is sensitive to the nature, structure and composition of the rocks is discussed, together with ways of identifying at depth rocks that are more prone to failure and those more prone to creep. It is also shown that pressure solution needs specific conditions to develop (presence of a fluid that may dissolve some minerals, specific pressure and temperature conditions to favour the maximum solubility of the mineral in solution). As a consequence, the whole geological context, and not only the lithology, should be considered.

2. Seismicity distribution and geology: the Vuache fault (Jura massif)

The first example is the Vuache fault, located in the Jura massif, within the western part of the Alps (Gratier et al., 1989; Lemoine et al., 1986). In this area, E–W Alpine contraction led to folds, thrusts and strike-slip faults that can be seen both in geological cross-sections and on maps (Fig. 1). The Jura massif is a typical foreland fold–thrust belt within this part of the Alps, where deformation affects a relatively thin sedimentary cover deformed above a basal décollement in Triassic evaporites (Hindle and Burkhard, 1999). The Jura belt was formed during the latest stage of the Alpine orogeny between the Upper Miocene and Lower Pliocene ages. It developed into a mountain range with arcuate folds-and-thrusts and strike-slip movement (major N–S to NW–SE sinistral, and minor E–W dextral strike-slip faults) that are linked with the Alpine arc formation (Affolter and Gratier, 2004). Present-day active faults are indicative of the continuity of tectonic loading with an active thrust fault being observed at the front of the Jura: ML 5.1 (local magnitude) 2004, Roulans earthquake (Cara et al., 2007; Molliex et al., 2011), close to Besançon and an active strike-slip fault in the rear part where occurred the ML 5.2 1996 Epagny earthquake (Hoang-Trong and Cara, 1998; Thouvenot et al., 1998), near Annecy. This latter earthquake occurred on the Vuache fault, which is one of the main NW–SE left-lateral strike-slip faults that currently offset the NE–SW trending folds-and-thrusts at the rear part of the Jura.

2.1. Seismicity distribution

The so-called Epagny earthquake is the strongest event recorded in southern-eastern France since 1962. The hypocentre was located in a Mesozoic limestone formation at very shallow depths (1–3 km). The focal mechanism indicates left-lateral strike-slip motion on a N136°-E-striking plane dipping 70° to the NE. This earthquake was followed by several hundred aftershocks, the locations of which were accurately determined thanks to the rapid installation of a temporary 16-station seismic network (Thouvenot et al., 1998). All aftershocks (magnitude 0.5 to 4) occurred along the southernmost segment of the Vuache fault, defining a 5-km-long, 3.5-km-deep, 130°E-striking rupture zone dipping 73° to the NE as the mean value (Fig. 2). However, some aftershock alignments appeared to indicate a more complex structure with some parts of the fault possibly being vertical. Fault-plane solutions for the 60-recorded aftershocks were consistent with left-lateral slip on a NW–SE striking plane. The intersection of the aftershock cluster mean plane with the topographic surface is very near the inferred extension of the Vuache fault marked on the geological map (Fig. 2). Aftershocks selected here (174 events) were well recorded by the temporary network, with more than 8 arrival times available, with an azimuthal gap smaller than 180°, and with high location accuracy: uncertainties are 160 m for epicentres, and 200 m for focal depths. Conversely, the main-shock position computed from permanent stations, up to 150 km away, was not as accurate as that of the aftershocks. However, by comparing the location of some aftershocks obtained from the local network with those obtained from the permanent network, it was possible to evaluate the location of the main earthquake with a horizontal uncertainty of less than 700 m.

2.2. Geological cross-sections

In order to compare the location of earthquakes at depth with the lithological characteristics of the sedimentary cover, geological cross-sections were constructed using both outcrops and drill hole data (Fig. 3). The balanced cross-section technique (Dahlstrom, 1969) was used to constrain the structures at depth as accurately as possible. This technique is based on the idea that a valid cross-section must be restorable to its initial state. This is achieved by assuming that the cross-sectional area is conserved during deformation above a single detachment fault and that at least some layers (competent layers) keep the same length over the entire deformation. In such case, a simple relation relates the transferred surface area (excess area above a reference layer) to the shortening (present length minus the initial length of a reference competent folded layer) multiplied by the depth of the detachment below the reference layer (Dahlstrom, 1969; Elliott, 1983; Hossack, 1979). The assumption of cross-sectional area conservation is supported by the observation of cylindrical folds perpendicular to the finite displacement with no evidence of strain extension parallel to the fold axis (except some fractures that account for no more than a few percent of deformation, which is considered here to be negligible). The balance between the excess area and the two other parameters (shortening and depth of the detachment) is based on a good knowledge of both the fold structure and the lithological section (Hossack, 1979; Ménard and

Please cite this article as: Gratier, J.-P., et al., Geological control of the partitioning between seismic and aseismic sliding behaviours in active faults: Evidence from the Western Alps, France, Tectonophysics (2013), http://dx.doi.org/10.1016/j.tecto.2013.02.013

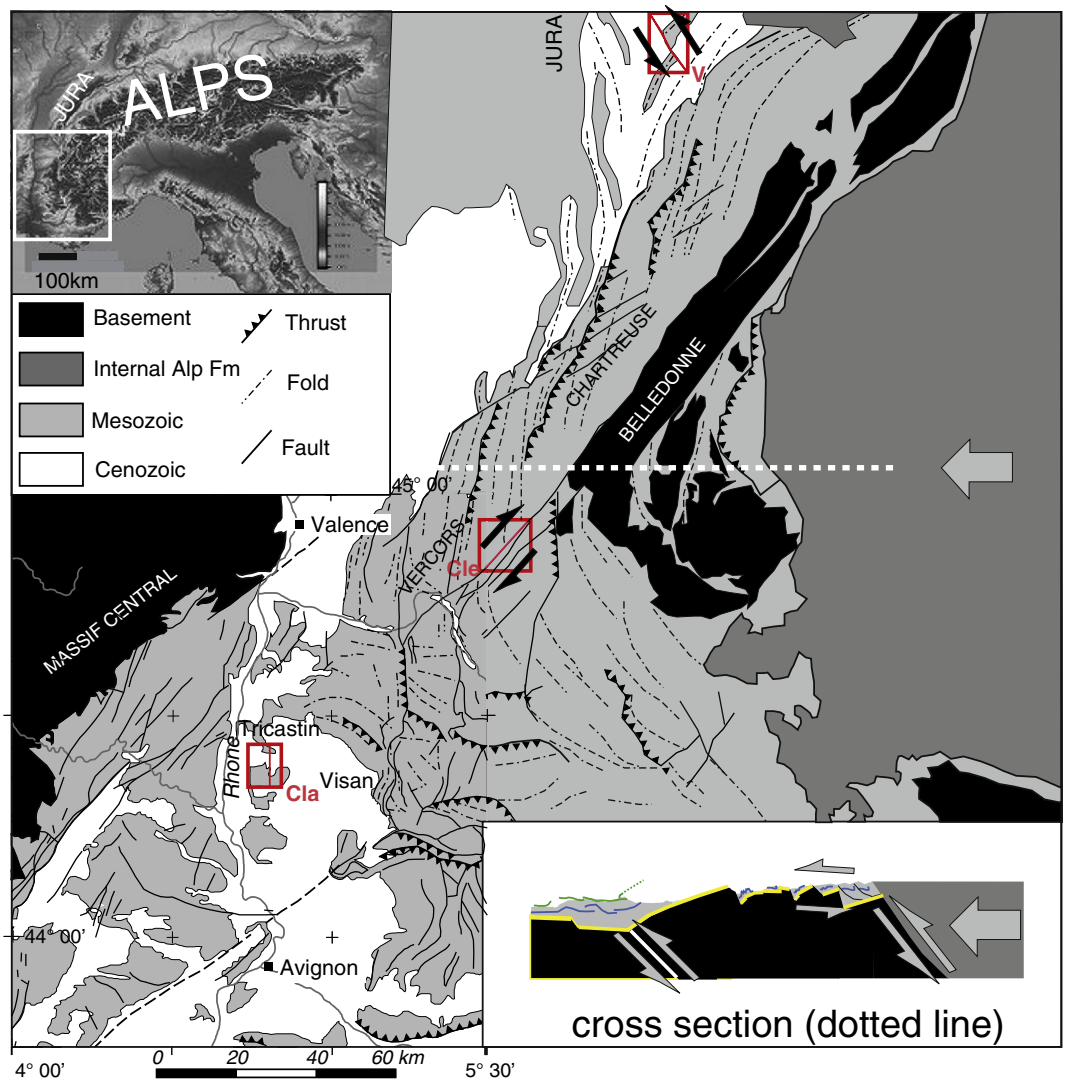

Fig. 1. Structural map of the western Alps (upper inset) showing the pattern of folds and faults and a general cross-section (Trias is in yellow, Tithonian in blue and Urgonian in green). The horizontal arrows indicate the main shortening direction during Western Alps formation. The upper part of the internal Alp boundary (Pennic Front) now shows extensional movement. The three zones studied are indicated with references to key locations: (V) the Vuache strike-slip fault, in the northern part (Jura massif), (Cle) the Cléry strike-slip fault in the central part (Vercors massif), and (Cla) the Clansayes normal faults in the western part in the Tricastin region, near the Rhône Valley Graben, and within the Visan syncline, adapted from (Gratier et al., 1989; Thouvenot et al., 2009). The lower inset show a cross-section oriented East–west. (For interpretation of the references to color in this figure, the reader is referred to the web version of this article.)

Thouvenot, 1987). The fold structures were drawn using data from outcrops, 1/50,000 geological map (Fig. 4a) and several drill holes. The lithological section was deduced from a neighbouring deep drill hole, located in Musièges, 8 km NW from the cross-section along the fault and completed for the lower Jurassic and Triassic parts by the Savoie-106 drill hole, 10 km west of Musièges (Donze and Enay, 1972). The lithological section goes through the whole sedimentary cover reaching the Triassic formations that form the detachment level below the deformation of the sedimentary cover and above the basement. Another drill hole (Humilly) located 18 km north of the cross-section was also used in order to estimate possible lateral variations (Affolter et al., 2008). The lithological section gives two types of information: the depth of the detachment (in the Triassic unit, Fig. 3a) below a reference layer (Urgonian limestone) and the thickness and geological characteristics of each unit of the sedimentary cover. An important issue is the reliability of the extrapolation of the Musièges drill hole to the studied area. Although lithological variations are described at a regional scale from the Jura Platform domain to the Subalpine domain (Deville and Chauvière, 2000), lateral variations are limited within the same domain. This can be seen when comparing two drill holes (Musièges and Humilly) 14 km away that show only slight variations (Affolter et al., 2008): the difference in thickness of the series from top-Urgonian to top-Trias is less than 5%. Consequently extrapolation of the lithology of Musièges to the studied area could lead to uncertainty on the depth of the various units of about 100 to 200 m. To obtain the best quantification of the change in lithology, the rock structure is described by a unique parameter, the mean thickness of the competent layers of limestone in a given unit (Fig. 3), evaluated from field observations. Given that the whole sedimentary cover is composed of a mixture of carbonate and phyllosilicate sedimentary rocks ranging from pure limestone to marl and calcareous mudstones, this unique parameter also characterizes the variations of the calcium content of the rock, that can also be considered as a simple indicator of the mean composition of the rock.

Two balanced cross-sections were constructed parallel to the active fault along the topographic surface (see Fig. 4a), using the 1/50,000 scale geological map of Seyssel (Donze and Enay, 1972). The fold axes are perpendicular to the finite displacement and no extension is seen parallel to these axes. This is compatible with balanced cross-section requirements. Outcrops in the cliff of the Mandallaz mountain (Fig. 4b)

Please cite this article as: Gratier, J.-P., et al., Geological control of the partitioning between seismic and aseismic sliding behaviours in active faults: Evidence from the Western Alps, France, Tectonophysics (2013), http://dx.doi.org/10.1016/j.tecto.2013.02.013

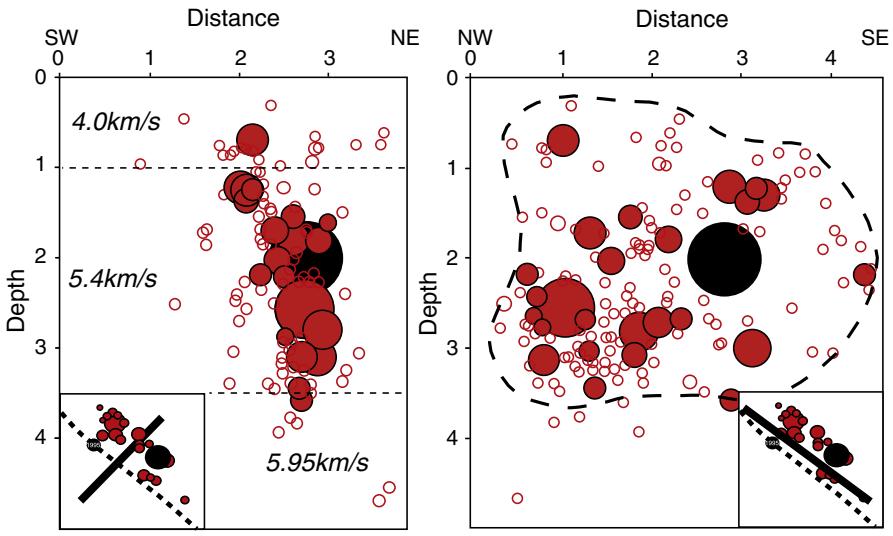

Fig. 2. The Vuache strike-slip fault: section through the aftershock zone, on the left a SW–NE section (with the velocity model), on the right a NW–SE section, black solid circle = main shock, red solid circles = aftershocks of magnitude 1 and more, open red circles = aftershock of magnitude less than 1. The thick dashed line is the inferred extension of the rupture area. Insets (map view) give the location of the cross-section (solid black line) relative to the geological trace of the fault at the surface (dotted line). Adapted from Thouvenot et al. (1998).

and two other (small) drill holes located along the southernmost cross-section provided additional constraints for the cross-sections (Fig. 4). A simple fault-bend fold can be drawn north of the fault, the shape being well constrained by the geological structures that can be seen on outcrops in the cliff that cuts the Mandallaz Mountain (Fig. 4b–d). This structure changes to a pop-up fold system south of the fault, with a shape being well constrained by two thrust faults found in the two drill holes located North and South of the pop-up fold (Fig. 4c).

2.3. Seismicity and geology

The active strike-slip fault separates two different structures. However, the earthquake location resolution was such that it was not possible to distinguish in which compartment (NE or SW) each event occurred. It should first be noted that the main-event rupture zone cuts through the whole sedimentary unit (Fig. 2). The locations of 25 earthquakes of magnitude equal or greater than 1.0 were projected on the geological cross-sections and are displayed on (Fig. 4c–d). Note that, with the exception of two events that occurred along the detachment level and which may be linked to some heterogeneity along this level, the main event and all the aftershocks are located in the massive limestone formations on either side of the fault. Events with a magnitude of less than 1.0 do not follow this observation. This may be explained by two reasons: (i) events of magnitude smaller than 1 are less accurately located than the larger ones; (ii) the size of the rupture area for an event of magnitude 0 to −1, which is typically in the 3–10 m range, is quite small and such events could have nucleated in thin limestone layers located within thicker marl sequences.

3. Seismicity distribution and geology: the Clansayes fault system (Tricastin region)

The Clansayes normal fault system is located in the middle of the Tricastin region (Fig. 1), in the western part of a large syncline structure (Visan syncline) that developed in successive steps from the Cretaceous Pyrénéo-Provencal (90 My) phase, up to the Alpine Cenozoic deformation (Miocene, 10 My) (Flandrin, 1975; Gratier et al., 1989). The active Clansayes normal faults are part of the normal fault system that developed later, towards the end of the Miocene (5 My), with sometimes a relatively large offset (up to 400 m), associated with the Rhône Valley graben development. This graben is part of the southern branch of the European Cenozoic rift system that dislocated western Europe, from the North Sea to the Mediterranean (Dezes et al., 2004).

3.1. Seismicity distribution

The Tricastin area has long been recognized as the site of earthquake swarms that are characterized by long series of shocks of various magnitudes with no outstanding principal events. The last earthquake swarm struck the region in 2002–2003, with a maximum magnitude of 1.7. The seismic activity was monitored for several months by means of a 16-station mobile network and this showed that the earthquakes were clustered along a NNW–SSE-trending, at least 5 km-long, shallow rupture zone, some foci being shallower than 200 m (Fig. 5, Thouvenot et al., 2009). An intriguing observation is the variation in focal mechanisms with depth. A composite focal solution built up from the observation of all events is rather difficult to analyse because of a number of first-motion polarities in wrong quadrants; however, a normal-fault mechanism with a slight strike-slip component emerges from it. Partitioning the whole set of earthquakes into three patches at various depths makes things clearer: events shallower than 200 m have almost pure strike-slip focal mechanisms, whereas deeper events have almost pure normal-fault mechanisms (Fig. 5).

3.2. Geological cross-section

A geological cross-section was constructed using both the 1/50,000 scale geological map of Valreas area and two drill holes (Visan and Pierrelatte), (Demarq and Bonnet, 1964; see Fig. 6a). The western end of the E–W Visan syncline can be seen on the WNW–ESE cross-section with the effect of the Pierrelatte normal fault. It should be noted that the Clansayes faults on the cross-section are simply deduced from the seismic activity and cannot be seen at the surface. The change in lithological characteristics (Fig. 3) was established using the lithological section given in the Nyons geological map (Flandrin, 1975).

3.3. Seismicity and geology

When plotting the number of events recorded during the swarm versus the lithology of the units (Fig. 6b), it is clear that most

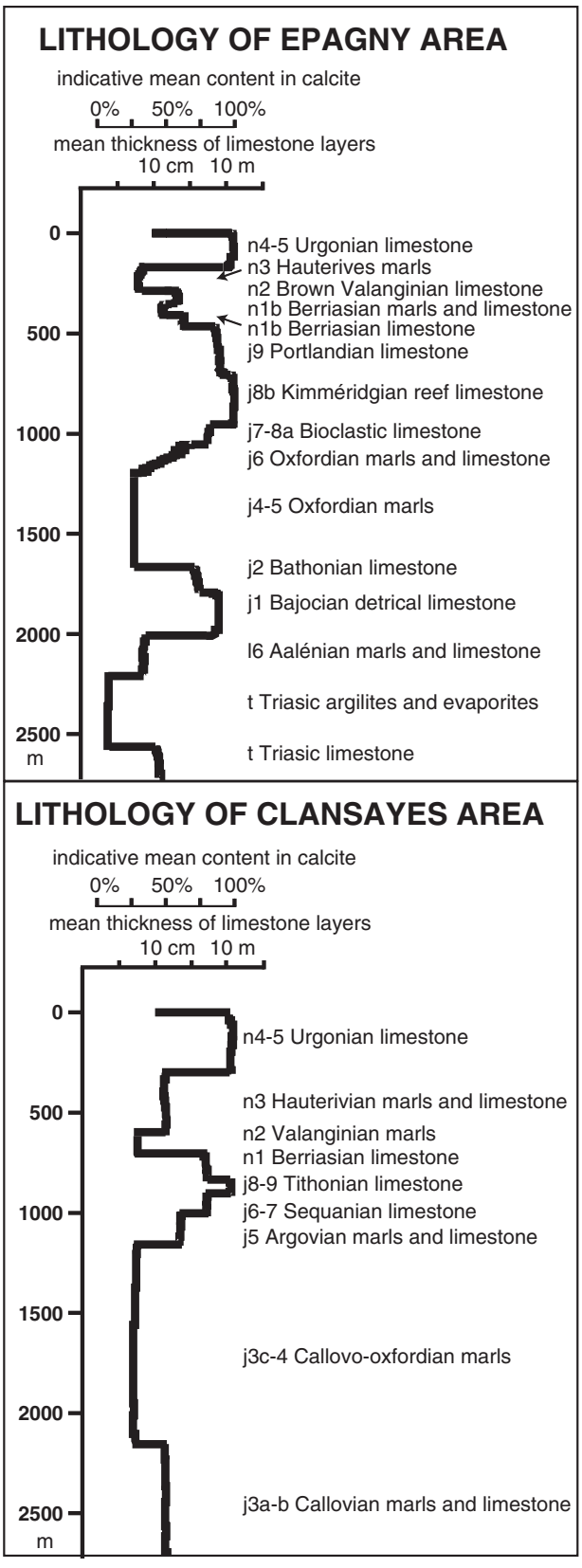

Fig. 3. Lithology of Epagny (Vuache Fault) and Clansayes areas: the mean thickness of limestone layers is plotted for each unit versus depth. Indicative calcite content is also given. The lithology of Epagny is drawn from the Musièges drill hole located less than 10 km from the rupture area (Donze and Enay, 1972). The lithology of the Clansayes area is drawn from the 1/50,000 scale geological map of Nyons (Flandrin, 1975).

earthquakes occurred in the Urgonian limestone located between 100 and 600 m depths. A few events are also associated with the Tithonian limestone located between 700 m and 1200 m depths. Both limestone formations represent thick sequences of marine carbonate deposits, with low porosity (0.6%) and quite high strength of 140 MPa estimated from uniaxial compression tests (Frayssines and Hantz, 2009), compared to other sedimentary units of the same area. As for the Vuache fault, but in a different tectonic context (normal fault instead of strike-slip fault), the occurrence of earthquakes of various magnitudes is observed to be fairly well correlated to the nature of the rocks: earthquakes initiate in pure and compact limestone formations.

4. Creep mechanism: the exhumed Cléry fault (Vercors massif)

4.1. Geological context

Having identified a clear correlation between earthquakes and rock composition (limestone to marl) at depths between 200 and 3000 m, the mechanism of creep in the weakest layers remains to be identified. The same sedimentary sequences as in the Vuache and Clansayes areas also outcrop in between: 130 km South-West and 80 km North-East respectively, near another recently exhumed strike-slip fault, the so-called Cléry fault (Fig. 1). In this case, it is possible to observe what happened at depth in the same geological context by looking at outcropping samples, which offers the opportunity to identify the creep mechanism. The depth of the deformation of the now outcropping part of the Cléry fault cannot have been deeper than the thickness of the stratigraphic serie above the transition between the Hauterivian marl and the Urgonian limestone, which is less than 1 km (Arnaud, 1975). The deformation occurred clearly near the end of Alpine age (Gratier et al., 1989).

The Cléry fault is located in the Vercors massif, which is part of the foreland fold–thrust belt of the western Alps. This massif probably began to form during the Miocene, associated with a large basement thrust of the Belledonne massif and above a detachment along the Trias level (Fig. 1) (Arnaud et al., 1974; Gratier et al., 1989). The main N–S fold and thrust system developed during this period and is sometimes crosscut by NE–SW dextral strike-slip faults that end up to the west against N–S syn-sedimentary normal faults. The right-lateral strike-slip Cléry fault cuts through the entire Vercors massif and represents the longest of these strike-slip faults. The total offset along the Cléry fault and the parallel La Selle fault (Fig. 1) was first estimated to be about 3–4 km based on measurements of the offset of sedimentary units (Arnaud, 1981). This value was confirmed later by measuring the difference in finite displacement between two cross-sections parallel to the faults (one north, the other south of the faults) that both end up against a N–S syn-sedimentary normal fault to the west: an offset value of 3.5 km was found by this method (Thibaut et al., 1996). It should be noted that the present day deformation in this western part of the Alps is probably accommodated mostly by strike-slip faults as attested by the active strike-slip fault in the Belledonne basement massif (Thouvenot et al., 2003), which is in the NE extension of the Cléry fault (Fig. 1).

A schematic geological map of the Cléry fault is given in Fig. 7 (Tourette, 2008), showing the location of the main fault, and a complex network of secondary faults. An associated fault network that developed around the main fault over a width of 500 m shows the common pattern proposed by Riedel (1929): conjugated R1 right-lateral and R2 left-lateral strike slip. The main displacement is located along the fault, with a decimetre-thick gouge in the Urgonian limestone. The limestone shows evidence of brittle faulting processes revealed by highly polished surfaces that are indicative of localized slip. Conversely, in the underlying marl unit (Fig. 7), a large shear zone of distributed deformation is observed, with a N–S pervasive cleavage pattern developing over a width of several hundred metres. This N–S cleavage is compatible with a shear zone in the marl that would be parallel to the main Cléry

Please cite this article as: Gratier, J.-P., et al., Geological control of the partitioning between seismic and aseismic sliding behaviours in active faults: Evidence from the Western Alps, France, Tectonophysics (2013), http://dx.doi.org/10.1016/j.tecto.2013.02.013

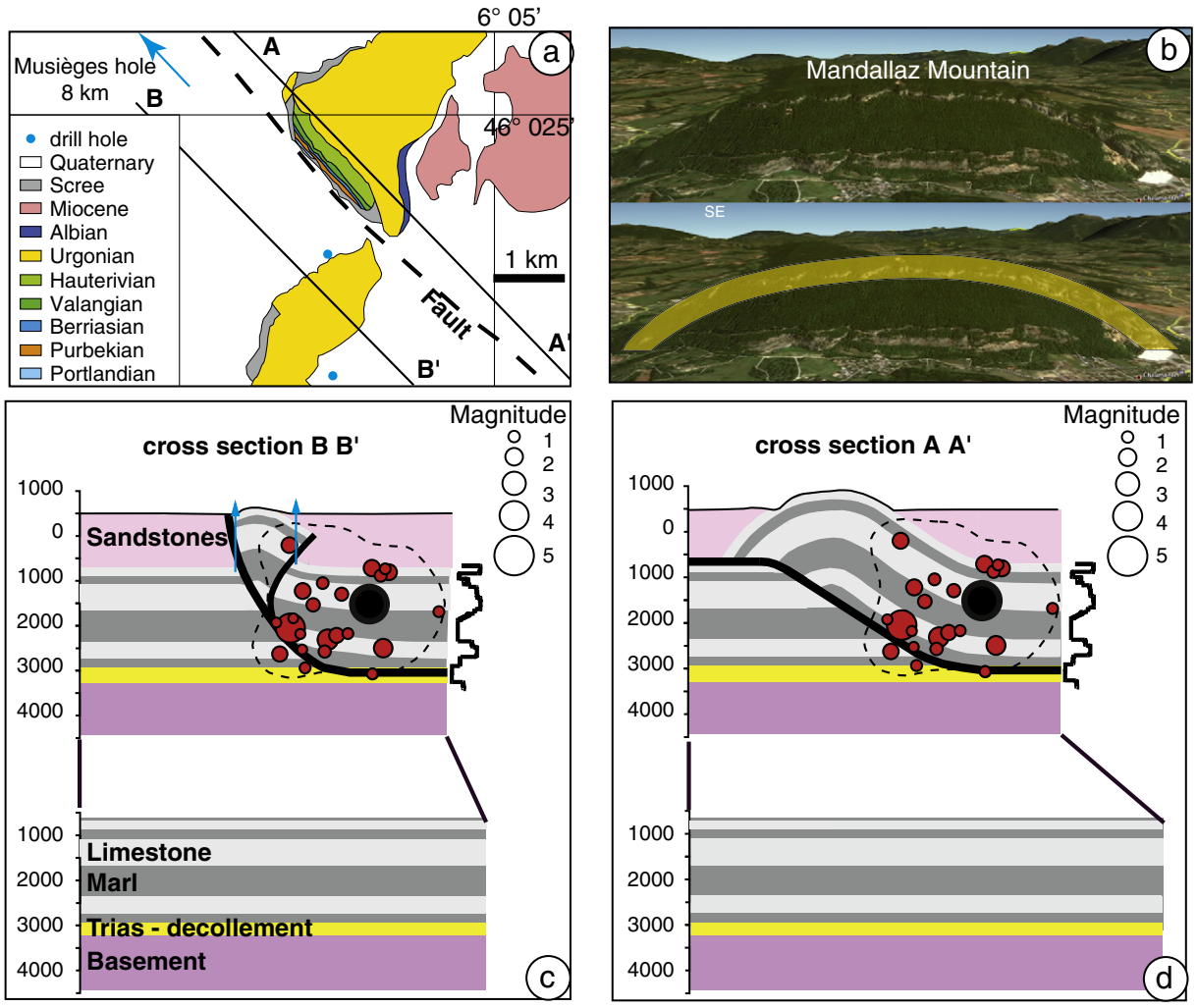

Fig. 4. Balanced geological cross-sections parallel to the rupture trace, Epagny area: (a) geological map and location of the three drill holes (blue dots); (b) view of the Mandallaz mountain showing in the cliff the shape of the thick Urgonian limestone folded layer; (c) section B B′ SW of the fault; (d) section A A′ NE of the fault. The restored cross-sections are given below both sections. In the two sections, on the top is the present day (deformed) state: the main shock (black) and the aftershocks of magnitude equal or larger than 1 are plotted with indication of their magnitude (from 1 to 5). All the events are located in limestone layers in one or other of the sections. Miocene sandstone is in pink, limestone in white, marl in grey, the Trias décollement in yellow and the basement in purple. (For interpretation of the references to color in this figure, the reader is referred to the web version of this article.)

fault in the limestone. These field observations point to the conclusion that, in the Cléry fault zone, the tectonic loading was accommodated by brittle deformation and fracturing in the strong limestone layers and by creep mechanisms in the weaker marl. The deformation mechanisms are identified and analysed in the following section.

4.2. Creep mechanism

The marl (Fig. 7) contains widespread spaced cleavages lying mainly N–S, obliquely to the fault, as commonly observed in shear zones (Fig. 8a, c, e). This shear zone is fairly wide: several hundred metres are centred on the main fault as can be seen on the map and on the cross-section (Fig. 7). Conversely the limestone exhibits various types of behaviour.

– Patches of polished fault surface are seen everywhere along the main fault (Fig. 8b), forming a network of segmented faults. Such brittle structures probably reflect the seismic behaviour of the fault by the presence of polished mirror-like striated surfaces (De Paola et al., 2012; Fondriest et al., 2012).
– The gouge is very narrow and follows the main fault (Fig. 7).
– The same N–S spaced cleavage as in the marl may be seen in the limestone, but the difference is that the width of the cleaved band is much narrower: just a few decimetres at most (Fig. 8d, f).

The mechanism of aseismic deformation may be inferred from micro chemical analysis of the samples. Evidence of pressure solution is revealed using elemental distribution maps obtained at various scales from X-ray fluorescence imaging of polished samples (centimetre scale) to EDS–SEM analyses (millimetre scale and below) on thin sections. Chemical element distribution maps are displayed in Fig. 9, for Ca, Al and Si; the brighter the colour the higher the chemical concentration. For both marl and limestone, the solution seams show both a Ca depletion zone and an Al and Si concentration zone. This is how the pressure solution creep process works (Gratier et al., 2013): starting from a rock containing both soluble (carbonates) and insoluble (phyllosilicates) minerals, the localized dissolution of a soluble mineral (in this case calcite) and the passive concentration of insoluble minerals (in this case phyllosilicates) lead to ductile deformation of the rocks (Fig. 9), as shown below. The cleavages in both marl and limestone are pressure solution cleavages (Fig. 9. However, as already said above, pressure solution creep is widespread over a much wider zone

Please cite this article as: Gratier, J.-P., et al., Geological control of the partitioning between seismic and aseismic sliding behaviours in active faults: Evidence from the Western Alps, France, Tectonophysics (2013), http://dx.doi.org/10.1016/j.tecto.2013.02.013

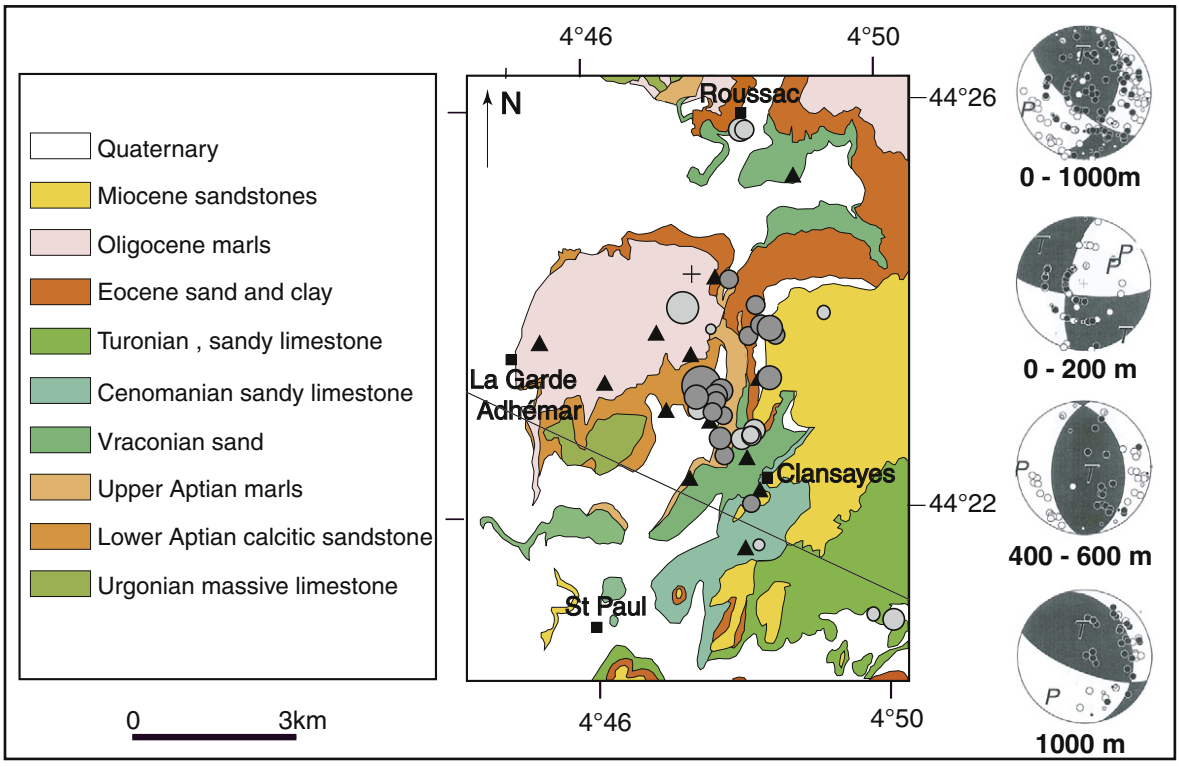

Fig. 5. Clansayes normal faults: on the left, the location of earthquakes is indicated on a schematic geological map, with lighter grey shade for events shallower than 200 m depth. Symbol size is proportional to the magnitude with a maximum value of 1.7. Solid triangles indicate the location of the seismological stations. On the right, a composite focal mechanism is given (top) with the variation in focal mechanism with depth (below).
Adapted from Thouvenot et al. (2009). (For interpretation of the references to color in this figure, the reader is referred to the web version of this article.)

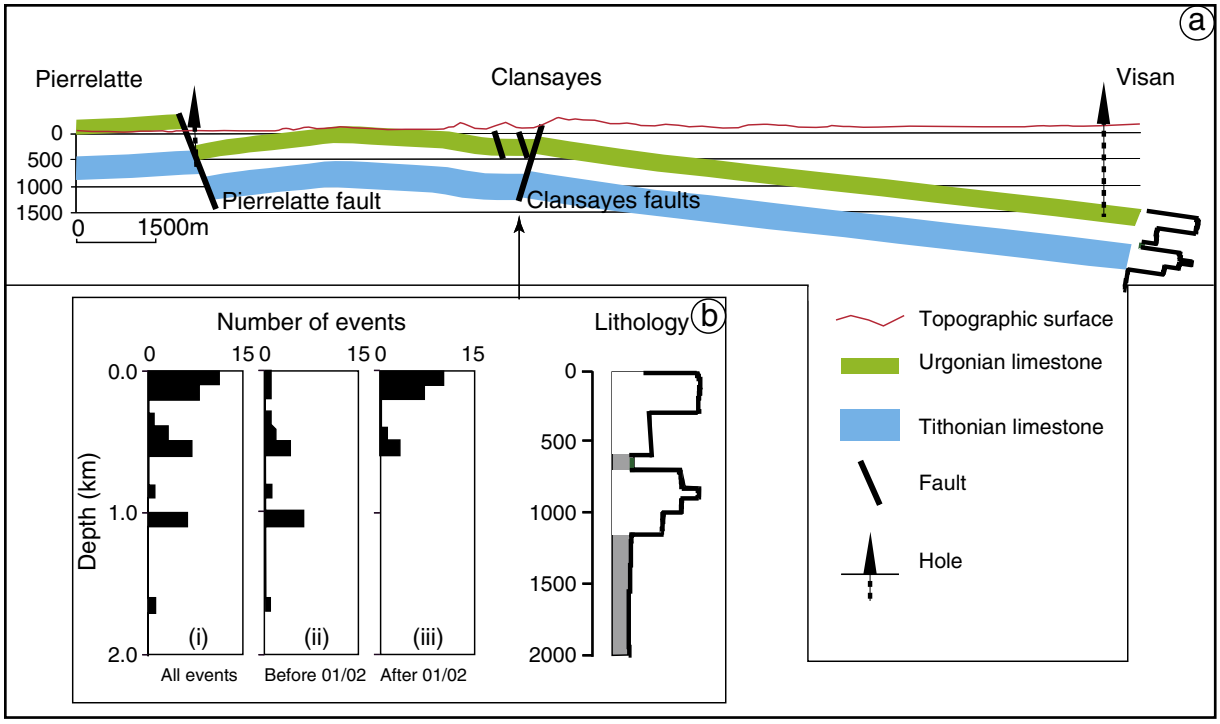

Fig. 6. (a) NW–SE geological cross-section through the Tricastin region (location in Fig. 5) showing the location of the two main limestone layers (see Fig. 3), the two drill holes, and the two sets of normal faults: Pierrelatte fault (deduced from drill hole) and Clansayes fault (deduced from earthquakes); (b) the inset on the left displays the number of events versus depth (all events) and a partition between events that occurred before or after the 1st of February. In parallel, a schematic view of the lithology is given (see Fig. 3) showing that almost all events are located in the limestone layers (white, 100–600 m). (For interpretation of the references to color in this figure, the reader is referred to the web version of this article.)

Please cite this article as: Gratier, J.-P., et al., Geological control of the partitioning between seismic and aseismic sliding behaviours in active faults: Evidence from the Western Alps, France, Tectonophysics (2013), http://dx.doi.org/10.1016/j.tecto.2013.02.013

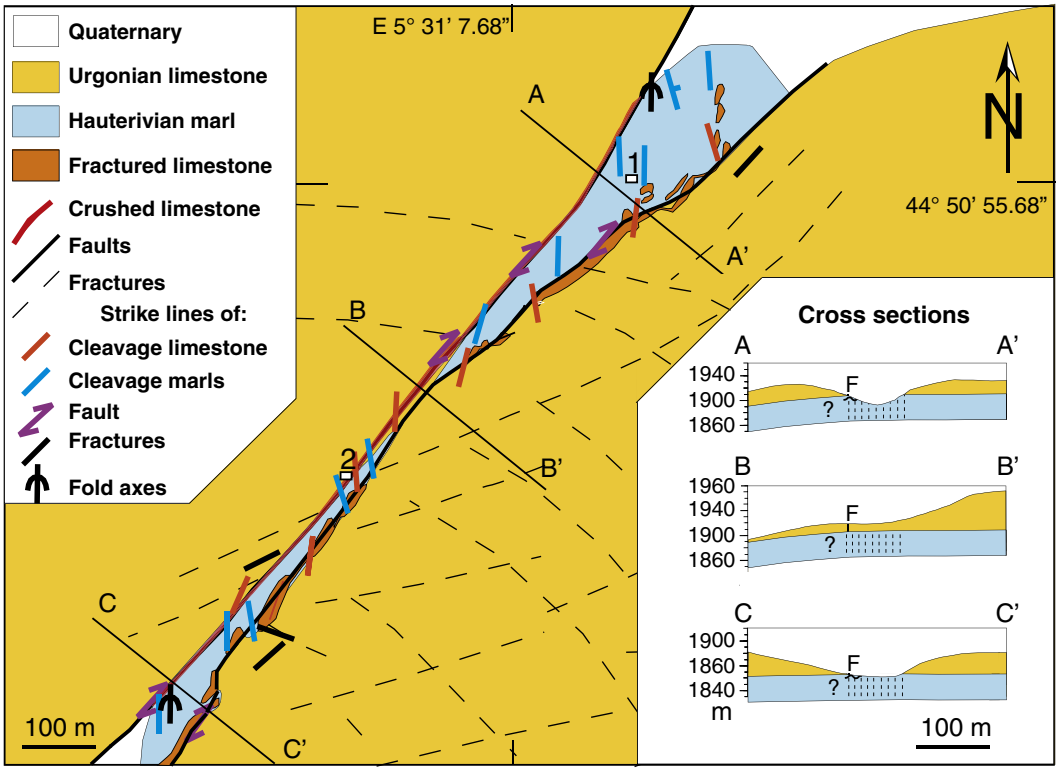

Fig. 7. Schematic geological map of the Cléry fault: limestone in yellow, marl with pervasive N–S cleavage in blue, deformed and cleaved limestone in orange. Fracture network (dotted line) is seen in the damaged zone of the limestone layer. Three geological sections show the relationships between fault and stratigraphic structures. References to key locations are given for the thin sections and outcrops of Figs. 8c–e and 9 (#1) and for the thin sections and outcrops Figs. 8d–f and 9 (#2). (For interpretation of the references to color in this figure, the reader is referred to the web version of this article.)

in the marl (hundred metres thick) than in limestone (decimetres thick) (Fig. 7). It should be noted that if widespread dissolution processes can be seen in both cases, attested by the dissolution seams (Fig. 9, labelled S), deposition veins are not so frequent even though it is possible to observe some (Fig. 9). Given this context, it is suggested that the deformation could have occurred in an open system with fluid flow through the fault zone washing away the soluble species. This is rather common in active creeping zones, as shown for example in the San Andreas Fault (Gratier et al., 2011; Mittempergher et al., 2011).

In more detail, however, pressure solution creep deformation patterns are rather different in marl and in limestone. In marls, permanent creep seems to occur. A question arises on the possibility that pressure solution creep may accommodate several kilometres of displacement. The answer depends on the possible strain values that depend on the width of the creeping zone and on the finite displacement. The order of magnitude of the finite displacement on the Cléry fault alone is about 2 km. A maximum width of 200 m can be seen with an asymmetrical position on the outcrop (Fig. 7). Depending on whether the shear zone is symmetrical or not, the minimum width may vary from 200 to 400 m. Consequently the simple shear strain (γ) may vary from 5 to 10 with for example the values of the principal strain shortening (l_1/l_o, l_1 = finite length, l_o = initial length) lower than 0.2 (Ramsay, 1967). The strain rate is even more difficult to evaluate. However if the displacement occurred over a period of 1 My, the strain rate could have been as low as 10^{-13} s^{-1}.

It must be noted that the angle between the solution cleavage and the creeping shear zone is not compatible with a passive rotation of the cleavage from 45° to for example 10° when $\gamma = 5$ (Ramsay, 1967). Angles between cleavage orientation and fault trend range between 20 and 45°. Consequently, one cannot consider that the cleavage is passively rotated during the creep process. More likely here the cleavage is developed and (at least partially) destroyed at each deformation increment as it is the case in incompetent layers for example in folding process when cleavage in incompetent layers remains perpendicular to the shortening all along the folding process (Ramsay, 1967). Such evolution is attested by the observation of various networks of cleavage that cross each other (Fig. 10, top). It is also the case in other creep zones such as in the San Andreas creeping zone (Gratier et al., 2011). Moreover, shortening perpendicular to solution cleavage cannot accommodate the large shortening value that is required with a large shear zone. The maximum value of shortening (l_1/l_o) associated with a solution cleavage process in marls or slates for example is about 0.5 (Gratier et al., 2013). Consequently we propose another mechanism of pressure solution creep, which is much more efficient: it is the mechanism of pressure solution diffusion-accommodated grain-sliding process. This mechanism has been proposed as superplasticity by Ashby and Verrall (1973). In their model the diffusion is accommodated by diffusion along dry grain boundary. Here one must consider that diffusion occurs along a thin fluid phase trapped under stress at the boundary of grains or domains. This mechanism can accommodate the very large strain value (l_1/l_o up to 0.2 or 0.1) that is required in creeping shear zones.

Conversely, the characteristics of pressure solution features in limestone are different from those in marls: as seen above, large deformation values may be accommodated in marls by grain (or domain) boundary sliding accommodated by pressure solution diffusion that occurs in a wide zone (several hundred metres), see Fig. 10, top. Conversely, in limestone one can see only spaced pressure solution cleavage that occurs within narrow creep zones (decimetre to metre in size), Fig. 10, bottom). The total cumulative displacement cannot be more than some metres, so earthquakes (or at least cataclastic deformation) must have to occur to accommodate the 2 km of displacement. Moreover, evidence of fracturing is seen all over this narrow creeping zones (see Fig. 10, bottom) and attest of the crucial interaction between fracturing and pressure solution:

Please cite this article as: Gratier, J.-P., et al., Geological control of the partitioning between seismic and aseismic sliding behaviours in active faults: Evidence from the Western Alps, France, Tectonophysics (2013), http://dx.doi.org/10.1016/j.tecto.2013.02.013

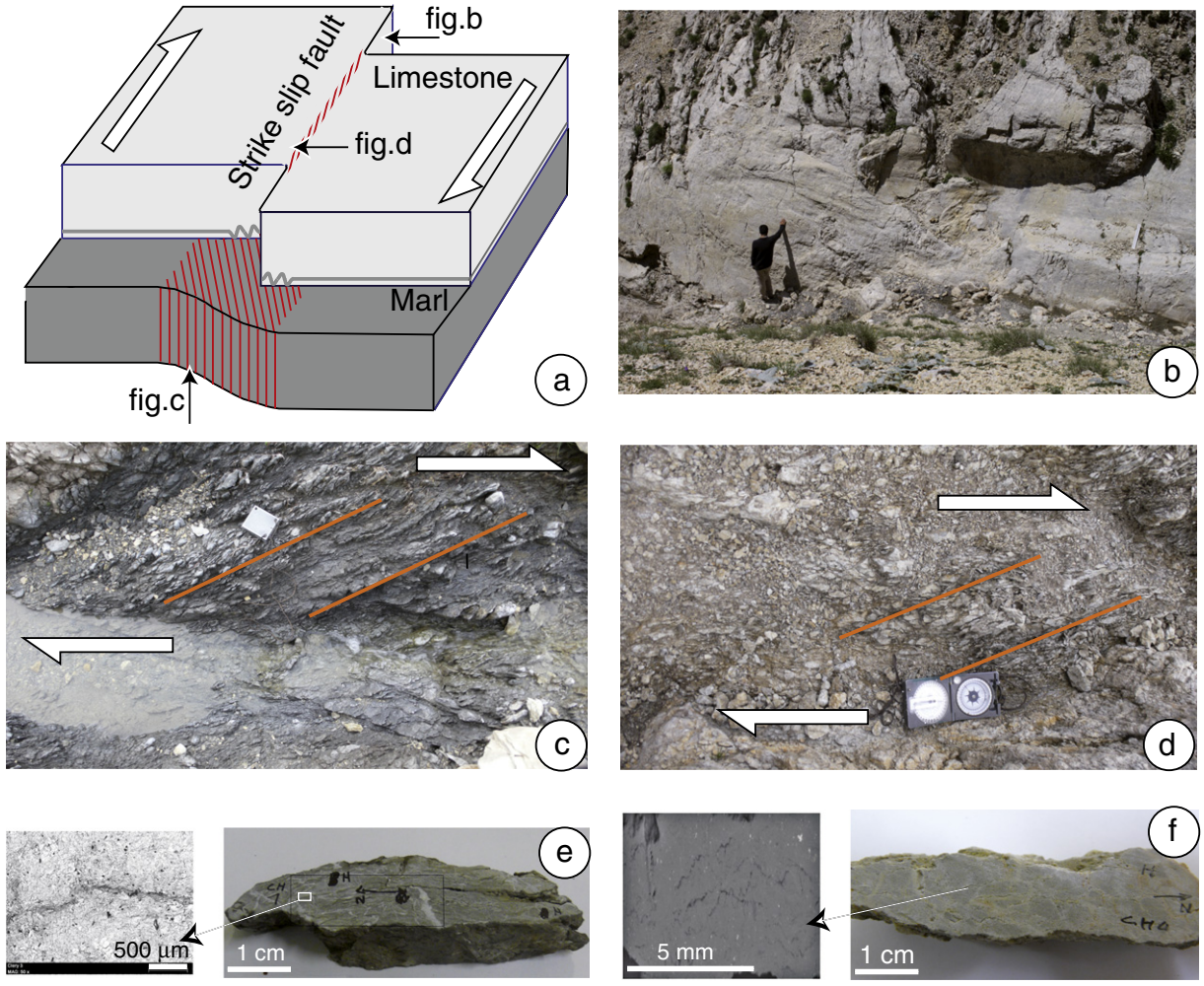

Fig. 8. Structural deformation patterns of the Cléry fault: (a) 3D synoptic model, sketch of limestone and marl layers with associated specific features (en echelon folds at the transition between the two main layers); (b) polished fault surface in limestone; (c) and (e) pervasive pressure solution cleavage at various scales from outcrop to thin section, loc. #1 in Fig. 7); (d) and (f) localized pressure solution cleavage band at various scales from outcrop to thin section (loc. #2 in Fig. 7).

fracturing accelerates pressure solution by developing a shortcut of diffusion, however, as fracture heals progressively this effect decreases with time and disappears (Gratier, 2011). Consequently, the pressure solution in limestone is episodic and accommodates only part of the total displacement.

5. Discussion

The answer to the question "could the partitioning between seismic and aseismic behaviours be controlled by the geological characteristics of the deformed rocks?" is clearly yes from all the examples studied, both from investigations at depth and from the study of the outcrop. It is clear that limestones are more prone to fracture and marls are more prone to creep along the same fault zone. In this specific example, which opposes the behaviour of limestone and marl, the first question is thus why does marl creep more easily by pressure solution than limestone since both contain the same soluble species, such as calcite? Another observation is that limestone may creep near active faults, and in this case the question must be "why does highly fractured limestone creep more easily that intact limestone rock"? Finally, it should also be pointed out that even though marl creeps, it is possible that, from time to time, a seismic event will pass through such rocks as was the case for the M5.3 Epagny earthquake that cut through the whole 3 km-thick sedimentary cover.

5.1. Why would earthquakes nucleate in limestone but not in marl?

The correlation of geological evidence with seismic relocation shows that earthquakes tend to localize inside limestones rather than marls in the areas of investigation of the present study. Several explanations may be proposed to explain this observation and to extend it to other context. They involved the two factors controlling strain: rheology and stress state.

A classical approach to the earthquake nucleation problem is the study of the parameters a and b of the empirical rate-and-state friction law (Marone, 1998; Scholz, 1998). If the difference $(a-b)$ is negative (velocity-weakening behaviour), fault frictional strength would decrease with increasing sliding velocity and a feedback loop would favour the sudden release of accumulated elastic stress along the fault. The fault would have a stick-slip behaviour. On the other hand, a positive $(a-b)$ coefficient (velocity strengthening behaviour) indicates that fault frictional strength increases with sliding velocity. If the fault accelerates, the higher friction would stabilize sliding along the fault.

Verberne et al. (2010) have shown that limestone gouges exhibit a transition between velocity-strengthening at low temperature (25–50 °C) to velocity-weakening behaviour at higher temperature (100–150 °C). Similarly, Ikari et al. (2011) undertook a series of systematic rate-and-state measurements. They confirmed the velocity-strengthening behaviour of Indiana limestone powder but showed

Please cite this article as: Gratier, J.-P., et al., Geological control of the partitioning between seismic and aseismic sliding behaviours in active faults: Evidence from the Western Alps, France, Tectonophysics (2013), http://dx.doi.org/10.1016/j.tecto.2013.02.013

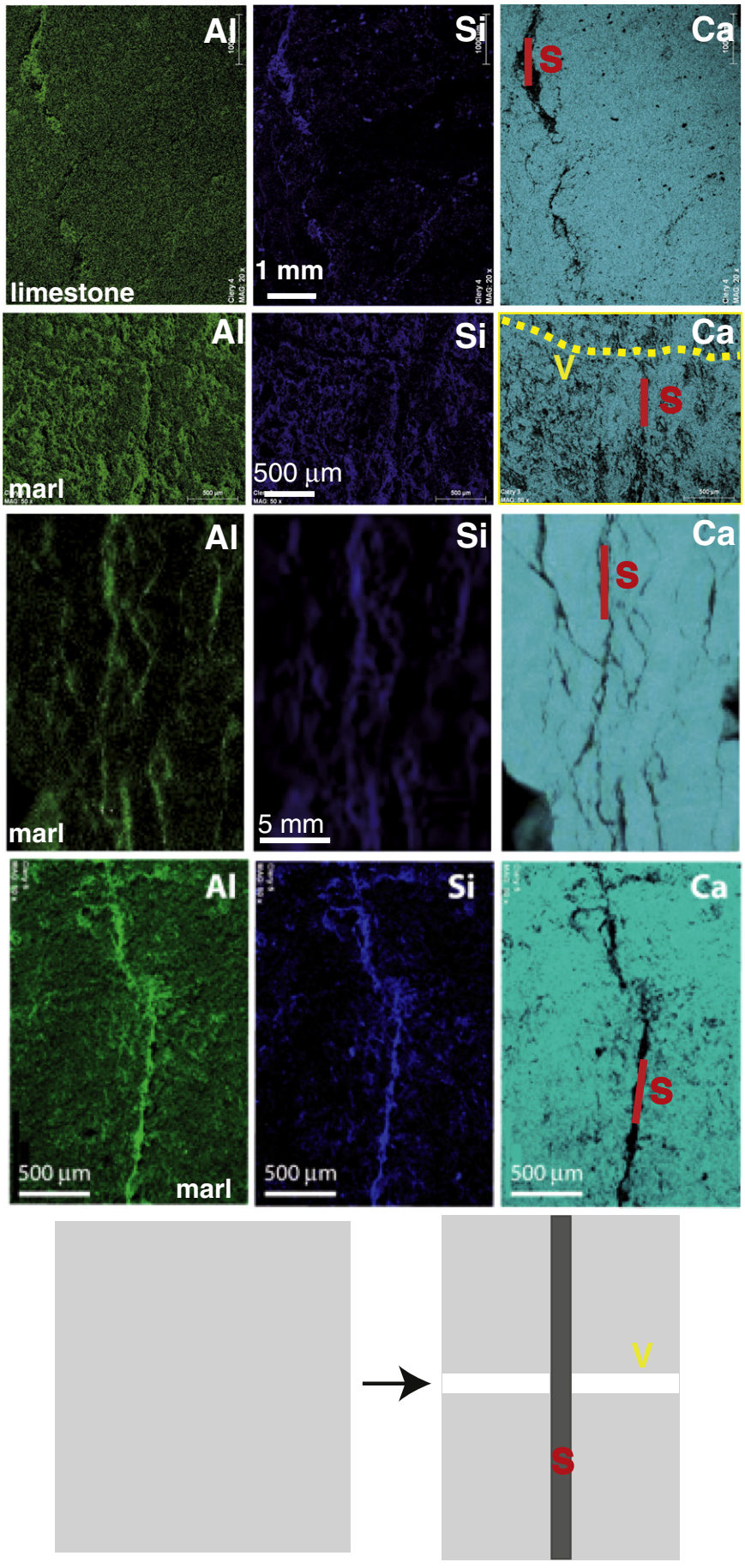

Please cite this article as: Gratier, J.-P., et al., Geological control of the partitioning between seismic and aseismic sliding behaviours in active faults: Evidence from the Western Alps, France, Tectonophysics (2013), http://dx.doi.org/10.1016/j.tecto.2013.02.013

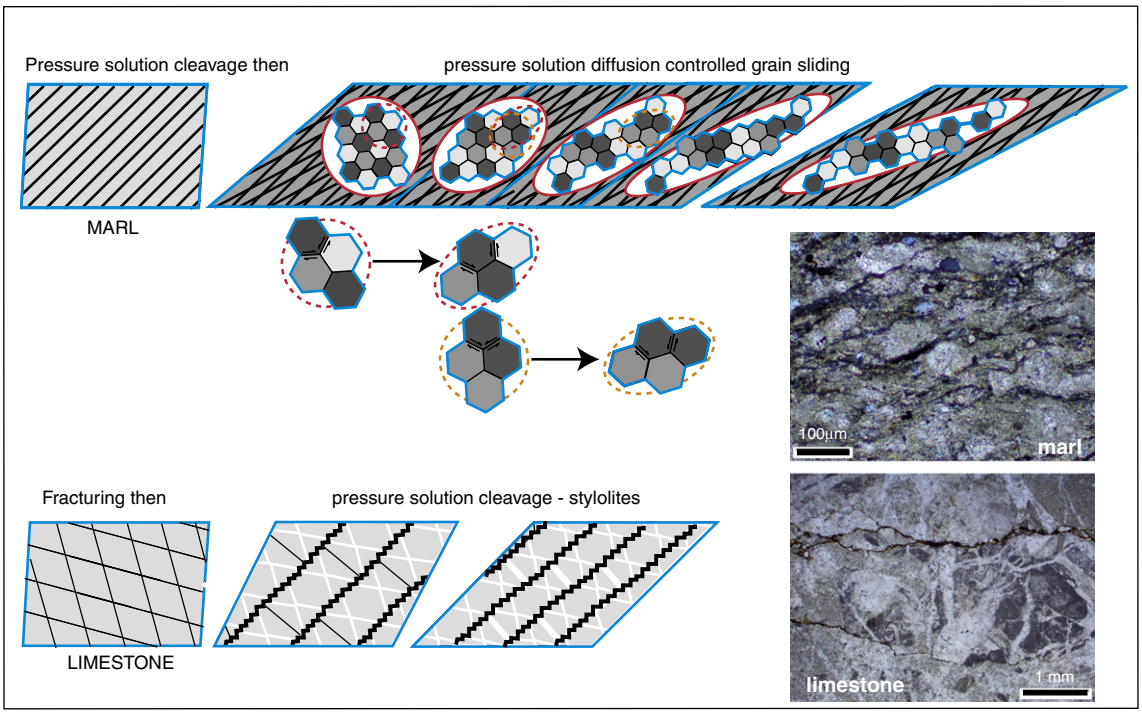

Fig. 10. Schematic observed evolution of pressure solution creep in marl and limestone: (top) evolution in marl: solution cleavage is developed and, at least partially, destroyed at each deformation increment, the large permanent deformation is accommodated by pressure solution diffusion-accommodated grain-boundary sliding; (bottom) evolution in limestone: solution cleavage developed locally associated with fracturing (black) and veins (white), accommodating only part of the deformation (post-seismic creep). On the right: view in thin sections of the two types of deformed rocks. (For interpretation of the references to color in this figure, the reader is referred to the web version of this article.)

that lithified limestone exhibits velocity weakening. This is consistent with field observations of sharp localization of slip within intact limestone (Fig. 9b), along the Cléry Fault, and the fact that the gouge accumulated more diffuse shear (Fig. 9d). However, there is no doubt from the Vuache and Clansayes faults that earthquake can initiate in limestone at less than 3 km depth. Thouvenot et al. (2009) clearly demonstrated that earthquakes can initiate in limestone at depth as low as 200 m. Rate-and-state experimental data are even less conclusive for shale. Lithified and powdered illite shale maintain a velocity-strengthening behaviour (Ikari et al., 2011) but smectite has a slip-weakening behaviour if the normal stress is below 40 MPa and the sliding velocity is slower than 20 µm/s (Saffer and Marone, 2003). The exact composition of the shale is therefore important in order to understand the frictional behaviour. The marl outcropping along the Cléry faults are illite-rich (but they contain also smectite and kaolinite minerals) and are therefore expected to have a velocity-strengthening behaviour, with little propensity to seismic sliding.

However, the velocity dependence alone is not fully predictive: the state of stress is also an important factor. Velocity-strengthening area can experience a high degree of slip, as recently observed with the Tohoku subduction earthquake of March 2011 where a large coseismic slip exceeding 40 m was observed along the décollement at the subduction toe (Ide et al., 2011). This has been proposed due to conditional stability where the slip becomes unstable under high dynamic loading (Lay et al., 2012; Scholz, 1998). Recent high velocity friction experiments have shown that clays can experience substantial weakening, especially by thermal pressurization (Wibberley and Shimamoto, 2005). Velocity-strengthening material located within a highly stressed environment can experience seismic activity. Hence, in addition to the intrinsic velocity weakening or velocity-strengthening behaviour, the energy accumulated within the system and possible fluid–rock reactions have to be considered. We will now discuss how variations in lithology also induce heterogeneity of the stress field. Both elastic and viscoelastic properties affect the stress state. A classical elastic model would predict that if alternating layers of marl and limestone were subjected to the same horizontal shortening ε_h, the resulting stress $\sigma_h = E\varepsilon_h$ would be higher in the stiffer limestone, which has a higher Young's modulus E, than in the marl. Other models taking into account erosion (MacGarr, 1988) would also predict variability in horizontal stress depending on the Poisson's ratio of the medium. The relationship between stress state and viscoelastic properties has been demonstrated by careful present-day stress measurements performed in Eastern France in a sedimentary cover with alternating argillite and limestone. Gunzburger and Cornet (2007) showed that the elastic theory did not predict the actual stress field. They could fit the different stress states in each lithology by invoking viscoelastic rheology. They found that stress is much smaller in the limestone layer that it should be according to experimental deformation. They concluded that limestone must deform permanently by some slow viscous process that is not reproduced in common experiments (that are most often much faster than geological processes). They suggested that such a viscous process could be a pressure solution creep that relaxes at least part of the geological stress. In the next part, we will discuss what controls the process of pressure solution.

Fig. 9. Pressure solution evidence: element distribution from Scanning Electron Microscopy (SEM) analyses at various scales and for various rocks: limestone (top) and marl (below). Brighter colours indicate higher content, for Al, Si and Ca elements. Cleavage seams (S) and calcite veins (V) are also indicated on the maps. Dissolution of calcite explains the low Ca content in the cleavage seams and is associated with passive concentration of insoluble species (Al and Si in phyllosilicates). The locations of the samples are given in Fig. 7: #1 as marl and #2 as limestone. Bottom is a sketch of the pressure solution mass transfer: (i) the initial state on the left is a polymineralic rock (light grey) with a mixture of soluble (white) and insoluble (black) minerals, (ii) the deformed state on the right shows the zone of passive concentration of insoluble species (pressure solution cleavage, S, dark grey) and a zone of re-deposition of soluble mineral (vein, V, white). (For interpretation of the references to color in this figure, the reader is referred to the web version of this article.)

Please cite this article as: Gratier, J.-P., et al., Geological control of the partitioning between seismic and aseismic sliding behaviours in active faults: Evidence from the Western Alps, France, Tectonophysics (2013), http://dx.doi.org/10.1016/j.tecto.2013.02.013

5.2. What are the key parameters of pressure solution creep laws?

In order to understand how rock composition controls pressure solution creep kinetics, an understanding of the key parameters of such creep mechanism is required. Pressure solution creep is a stress-driven mass transfer process involving three kinds of parameters (Gratier et al., 2013):

i) The driving force, which is the difference in chemical potential of the solid between the dissolution zone and the deposition zone, causing mass transfer through the fluid phase trapped under stress (Paterson, 1973; Weyl, 1959).
ii) The kinetics of the process, implying three successive steps: dissolution, transfer and deposition. As in all in-series processes, if the rate of a given step is much slower than the others, then it controls the rate of the entire process and corresponds to a specific creep law. This means that several pressure solution creep laws are possible (Bos and Spiers, 2002; Raj, 1982) depending on the limiting step.
iii) The mass transfer mechanism, either diffusion or infiltration, carries the soluble species from dissolution to deposition sites and controls the length scale of the process (Lehner, 1995).

In most pressure solution processes in natural deformation, one step of the in-series process is diffusion through a fluid phase, which is trapped under compressive stress. In this case, the diffusion flux (product of the diffusion and the thickness of the diffusive pathway) along such a trapped fluid phase is always very slow compared with a diffusion flux in a free fluid with large pores or open fractures that may be part of the diffusive path (with a much wider diffusive pathway). So when most of the diffusive transfer occurs through trapped fluids, as in the case of deformed rocks with very low porosity, the kinetics is controlled by the diffusion along the fluid phase trapped under stress. There are some exceptions: pressure solution of quartz is known to be dissolution-limited at a low temperature, below 150 °C (Bjorkum et al., 1998) but is controlled by diffusion at a higher temperature (Gratier et al., 2009). Specific impurity elements in solution that slow down interface reaction may render pressure solution of calcite (Zhang et al., 2010) or quartz (Bjorkum et al., 1998; Bjorlykke and Hoeg, 1997) limited by the reaction kinetics.

Assuming that the kinetics is controlled by diffusion, a general relationship relates the axial strain rate of a cylinder of height d with the axial stress and the other parameters as follows (Gratier et al., 2009):

$$\dot{\varepsilon} = d\Delta d/dt = 8DwcV_s\left(e^{3\sigma_n V_s/RT}-1\right)/d^3 \quad (1)$$

where d is the distance of mass transfer along the thin fluid phase trapped under stress (diameter of the cylinder), t is time (s), c is the solubility of the diffusing solid ($mol \cdot m^{-3}$), V_s is the molar volume of the stressed solid ($m^3 \cdot mol^{-1}$), R is the gas constant (8.32 $m^3 \cdot Pa \cdot mol^{-1} \cdot K^{-1}$), T is the temperature (K), D is the diffusion constant along the stressed interface ($m^2 \cdot s^{-1}$) and w is the thickness of the fluid interface (m) along which diffusion occurs. σ_n is the driving force: the difference between axial normal stress on the dissolution surface and normal stress on the precipitation surface (often corresponding to the fluid pressure around the cylinder). The constant 3 in the exponential of Eq. (1) takes into account the fact that, in order to balance forces during a constant approach of two planar surfaces, the normal stress at the centre of the contact between the surfaces is higher than the average stress across the contact (Dewers and Ortoleva, 1990). The stress relation may also be expressed as a power relation at high stress instead of the exponential relation: ${\sigma_n}^n$ with $n=1.75$ (Gratier et al., 2009). A linear relationship ($n=1$) may be considered as a good approximation if the driving stress is low enough (less than 30 MPa), (Rutter, 1976). In conclusion, pressure solution flow law includes various parameters: solubility of the minerals in solution, diffusion flux along the dissolution contact and stress. The creep rate is inversely proportional to the diffusion distance along the fluid phase trapped under stress. From a more general point of view, pressure solution mechanism is always associated with a slow strain rate (less than 10^{-10} s^{-1}) and a relatively low differential stress. It competes in the upper crust with brittle creep and cataclastic frictional (seismic) processes that need much higher differential stress values. Both mechanisms are overridden by aseismic dislocation glide deformation processes at temperatures higher than 400–500 °C.

5.3. Why does marl creep more easily by pressure solution than limestone?

Both marl and limestone contain a soluble species, carbonate minerals (mainly calcite). However, marl is a polymineralic mixture of soluble (about 50% calcite) and insoluble minerals (about 50% clays and phyllosilicates) and limestone is monomineralic, made up of almost 100% calcite. Some parameters of the creep law (Eq. (1)) are the same for the two types of rocks. The imposed displacement rate is the same. Other parameters such as solubility, molar volume, are of course the same in limestone and marl since they relate to the same soluble calcite mineral. The stress depends on the possibility of deformation: if the rock creeps, this lowers the differential stress level; if it does not, the stress is likely to increase, leading to rupture. So, it is difficult to assess the stress level. However, from observations made, marl creeps more easily than limestone, so the differential stress level must be lower in marl than in limestone. The mass transfer distance is not fundamentally different even if it is likely that marl has a smaller grain size than limestone. There is, however, a difference that has been shown in several studies: monomineralic rocks, composed of 100% soluble minerals are always more difficult to deform by pressure solution than polycrystalline rocks with a mixture of soluble and insoluble minerals. This has been shown in the field where veins made of 100% calcite or quartz act as rigid objects when embedded in marl or shale formations (Gratier, 2011). This has also been shown by experiment: (i) dissolution and diffusion out of stressed wet contact occurs more easily at contacts between different minerals than at contacts between the same minerals (Hickman and Evans, 1991; van Noort et al., 2007); (ii) aggregates with soluble species contents ranging from 45 to 75% dissolve faster than aggregates with 100% soluble minerals (Zubtsov et al., 2004). The reason for this is that, in the case where there is a mixture of soluble and insoluble species, the soluble species diffuses relatively easily at the contact between two different minerals; consequently pressure solution creep for polymineralic rocks may be efficient (Fig. 11a). Conversely, with monomineralic rocks, grain contacts are between the same minerals (calcite, quartz…) and in this case there is very often a possibility of healing that has been shown to slow down drastically the diffusion flux (Fig. 11a). In this case, the pressure solution creep rate for monomineralic rocks is much slower than for polymineralic rock, with all other conditions being the same. This does not mean that monomineralic rocks cannot creep: evidence of pressure solution in limestone can be seen on the field (Andrews and Railsback, 1997; Bauerle et al., 2000; Heald, 1955) and has been demonstrated from in situ stress measurements (Gunzburger and Cornet, 2007), but their viscosity is higher than for polymineralic rocks, with all other conditions being the same.

5.4. Why does highly fractured limestone creep more easily by pressure solution than intact limestone?

Our field observations show that pressure solution creep can develop in limestone, through spaced pressure solution seams, along very narrow bands parallel to the fault (Figs. 7 and 8). The reason why the creeping process is so localized merits an explanation. As already discussed, with all parameters being the same in Eq. (1) for a

Please cite this article as: Gratier, J.-P., et al., Geological control of the partitioning between seismic and aseismic sliding behaviours in active faults: Evidence from the Western Alps, France, Tectonophysics (2013), http://dx.doi.org/10.1016/j.tecto.2013.02.013

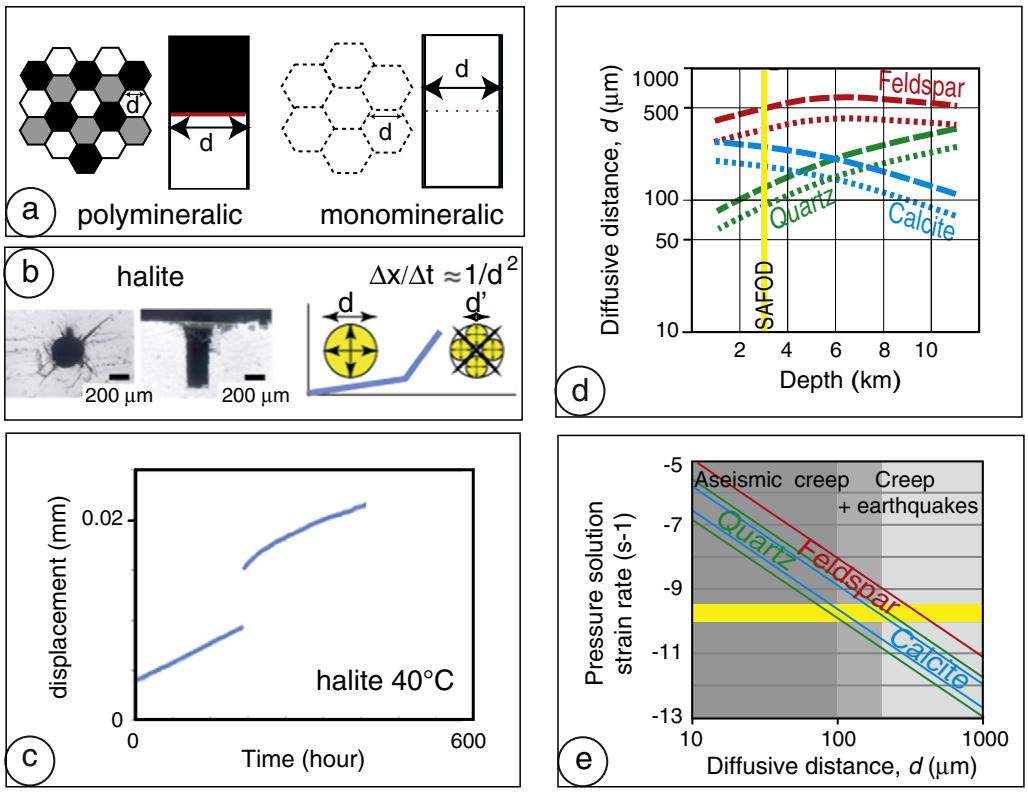

Fig. 11. Creep mechanism: (a) sketch of the difference in mass transfer paths between polymineralic rock (diffusive paths along two different mineral grain boundaries) and monomineralic rock (diffusive path along clouds of fluid inclusions linked to the healing of identical mineral grain boundaries); (b) mechanism of fracture-induced deformation weakening: during indentation of halite by dissolution under stress, a dramatic change in displacement occurs when radial fracturing develops, the effect of the fracture being to reduce the mean mass transfer distance along the trapped fluid under the indenter from d (indenter diameter) to d' (mean spacing between fractures), adapted from Gratier (2011); (c) variation in displacement rate after fracturing by dynamic loading that triggers the displacement rate (see b) and progressive strengthening due to fracture healing, adapted from Gratier et al. (2013); (d) distance of diffusive mass transfer d versus depth for various minerals required to accommodate 20 mm/yr horizontal displacement rate by pressure solution creep in vertical shear zones of 1 m width (dotted line, strain-rate of 3.3×10^{10} s^{-1}) or 3 m width (dashed lines, strain rate of 1.1×10^{10} s^{-1}); (e) pressure solution strain rate versus distance of diffusive mass transfer through the whole crust for various minerals, minimum and maximum values for quartz and calcite, maximum value for feldspar, yellow line is the required strain rate for the creeping zone.
Panels (d) and (e) adapted from Gratier et al. (2011). (For interpretation of the references to color in this figure, the reader is referred to the web version of this article.)

given limestone, there are only two parameters that can vary spatially. While stress levels may vary laterally, it is unlikely that this would lead to such a localization process. Another parameter of a much greater importance is the mass transfer distance (d in Eq. (1)). If a damaged zone develops along the gouge, as seen in most fault zones, fracturing drastically reduces the mass transfer distance. This effect has been demonstrated by dynamic indenting experiments (Gratier, 2011). The principle is to place a sample in contact with a saturated solution and to press it with a small indenter loaded with a constant dead weight over a long period (weeks or months). Then, from time to time, a steel ball is dropped on the deadweight to mimic the dynamic shaking felt during an earthquake. The strain rate is measured permanently with three high-resolution displacement sensors. For example, when working on halite minerals at 40 °C nothing happens in dry conditions, indenting occurs only in the presence of the mineral solution reflecting the pressure solution process. The drastic effect of the ball modifying the displacement rate for halite can be seen in Fig. 11c: the displacement rate increases instantaneously then slowly decreases with time (over a period of several weeks of months). This can be explained by looking at the sample after the experiment (Fig. 11b): radial fracturing is promoted during dynamic loading. This fracturing induces diffusion short cuts for the diffusive mass transfer along the thin fluid film trapped under the indenter as the fractures are a thousand times wider than the thickness of the fluid phase trapped under the indenter. The mass transfer distance changes from the size of the indenter (d) to the spacing between the fractures (d'), Fig. 11b. As diffusion is rate limiting in this case, and as the displacement rate is thus inversely proportional to the square of the mass transfer distance, it is clear that reducing the mass transfer distance increases the displacement rate. In nature both fracturing and cataclasis may reduce the distance of mass transfer (Jefferies et al., 2006). It should be noted that, in the laboratory, as in nature, the fractures are progressively sealed, so after some time they stop activating diffusion. Consequently, the displacement rate progressively decreases with time after a seismic slip in the field (Freed, 2007) and after a shock in the lab (Fig. 11c). It is not possible to discuss such time-dependent variations on our geological examples. It will simply be considered here that seismic fracturing accelerates pressure solution by reducing the mass transfer distance and this explains the tight localization of the post-seismic creeping zone in limestone.

5.5. Could other types of rock creep by pressure solution in subduction zones?

In subduction zones the main minerals are most often quartz, feldspars, serpentines and phyllosilicates. We discuss here how to extend the results obtained with carbonate/phyllosilicate mixture to quartz and feldspar/phyllosilicate mixture. It is well known that several minerals are soluble under stress and can contribute to pressure solution creep. In natural deformation, pressure solution is a major mechanism of deformation of calcite and dolomites (Andrews and Railsback, 1997; Bathurst, 1971; Carrio-Schaffhauser et al., 1990), quartz (Heald, 1955; Wangen, 1998; Weibel and Keulen, 2008), feldspars (Gratier et

al., 2011; Thomas et al., 1993), gypsum and halite (Bauerle et al., 2000) and serpentine (Andreani et al., 2005). So every rock containing at least one of these minerals can deform by pressure solution especially if, as seen above, it also contains some phyllosilicate minerals or is highly fractured. In subduction zones quartz, feldspars, serpentines are found with often a minor amount of carbonates. The efficiency of pressure solution deformation is strongly dependent on the solubility of the mineral in solution, which itself depends on the thermodynamic conditions. For example, at 25 °C, the solubility in water of the main minerals involved in pressure solution creep decreases from halite to gypsum, calcite, feldspar and quartz. Conversely, at 300 °C, feldspar and quartz have a much higher solubility than, for example, calcite or dolomite and are therefore much more mobile under stress (Gratier et al., 2013). The role of pressure solution has been demonstrated in the steady state creep of the San Andreas Fault creeping section associated with some microseismicity (Holdsworth et al., 2011; Schleicher et al., 2009). Samples were retrieved from the SAFOD drill hole and pressure solution creep was revealed by microprobe analysis (Gratier et al., 2011; Hadizadeh et al., 2012). The soluble species are quartz, feldspars and calcite. The insoluble species are mostly phyllosilicates. A deformation map of the three main minerals (calcite, feldspar and quartz) has been proposed by Gratier et al. (2011) (Fig. 11d) assuming a near-constant driving force at depth, as observed from measurements in the drill hole (Zoback et al., 2010). An increase in stress with depth could lead to a slightly different pattern (Gratier, 2011; Rutter, 1976). The same effect of the presence of clay mineral is seen for polymineralic rocks: a mixture of quartz plus clay is always more likely to accommodate stress by creeping compared to a massive vein of quartz (Niemeijer and Spiers, 2005). Consequently, competent quartzites or sandstones are more likely to be the site of earthquake initiation than other rocks like schist (mixture of quartz and phyllosilicates).

The effect of the nature of rocks on the seismic–aseismic transition has been proposed in other studies. For example, the Indian plate slips aseismically beneath the wide plateaux fronting the Kohistan Mountains along an aseismic viscous salt detachment (Satyabala et al., 2012). Deformation partitioning between aseismic creeps along the bedding-plane, inter-bed sediment detachment and seismic deformation located in the thrust ramps through the more rigid basalt flows, have also been observed in the Columbia River (Wicks et al., 2011).

5.6. How do creeping zones act as barriers to earthquake propagation?

In areas where some fault patches slip aseismically and other patches slip seismically, some of the continuously creeping patches may act as barriers to the propagation of neighbouring earthquakes (Perfettini et al., 2010). The idea is that, since creep relaxes stress, there is a smaller amount of shear stress to be released in earthquakes in aseismically creeping areas (Collettini et al., 2011). However, as said above, it all depends on the efficiency of the creeping process. As pressure solution is a viscous process that strongly depends on loading rate, the creeping process may relax the stress continuously; in such a case, the steady-state creep process may be maintained. Conversely, the stress may not necessarily be completely relaxed and may continue to rise even in case of creep. This may be due to an effect of the nature of the rock or the lack of fluids. However, even for the same type of rocks it may also be just the effect of the mass transfer distance (the mean distance between fractures or the grain size, Gratier et al., 2011) (see Fig. 11e). In this case, the progressive increase in stress value in a creeping segment will lead to rupture. An example of this behaviour can be seen along the Hayward fault in the San Francisco Bay Area. This fault exhibits significant aseismic creep during the interseismic phase of the seismic cycle. A strongly coupled asperity was identified by geodetic data, corresponding to the mapped surface trace of the 1868 M6.9 Hayward earthquake. The fault is embedded in gabbroic rock that is less likely to creep than neighbouring rock formations. In this case, earthquakes seem to initiate in the segment that is creeping at the lowest rate (Evans et al., 2012). As stated by Collettini et al. (2011), when a crustal fault zone contains a mixing of weak creeping material and of relatively strong non-creeping lenses, continuous creep concentrates stress around and within the strong potentially unstable lenses which may lead to earthquake nucleation. However, the problem is even more complex since the dynamic propagation of a neighbouring earthquake could also break the barrier even if the stress level is very low. In this case, by looking at the aseismic sliding fraction that occurs between earthquakes, and by taking into account distance, time and sliding speed (Perfettini et al., 2010), it is possible to determine whether an earthquake that begins in one locked area is likely to stop when hitting an aseismic barrier, or whether it will be able to cross that barrier and propagate the rupture on the other side.

5.7. Which criteria could be used to identify geological control on the transition between seismic and aseismic slips at depth in subduction zones?

There are several techniques available for distinguishing creeping zones from non-creeping zones at depth. The first is geodetic measurements. However, it is always difficult to distinguish elastic loading from irreversible deformation. Long-term measurements are needed with high spatial resolution. Even so, they could at least give a general view of seismic versus aseismic behaviour. In subduction zones, for example, such measurements have been taken to evaluate the sliding part that is accommodated either by seismic or by aseismic deformation. It has been shown that, in Peru, 50% of slip in the seismic–aseismic transition range is actually aseismic (Chlieh et al., 2011). In western Canada, according to Mazzotti et al. (2011), long-term regional aseismic deformation may account for a significant part of the deformation and, in some areas, may represent as much as 90% of the total deformation budget. In eastern Japan, aseismic zones are also well identified by geodetic measurements, such as for example the Sanriku-Oki low-seismicity region that accommodates aseismic convergence along the northern margin of the 2011 Tohoku-Oki earthquake rupture (Ye et al., 2012).

The P- and S-wave velocities may also be investigated. For example, a thin layer (some hundred metres thick) was found to have low P-wave velocity (3–4 km/s) at the top of the plate boundary in Japan and corresponds to aseismic material. When comparing the distribution of relocated hypocentres with a tomographic image of the Northeast Japan forearc it has been shown (Zhao et al., 2011) that the rupture nucleation of the largest events in the Tohoku-oki sequence, including the mainshock, was controlled by structural heterogeneities in the megathrust zone. The 2011 Tohoku-oki earthquake and other major shocks initiate in the zones of high P-wave velocity. Conversely, low velocity zones in the megathrust zone may contain subducted sediments and fluids associated with slab dehydration (Zhao et al., 2011) that are likely to slip aseismically. Extremely low P-wave velocities along the plate interface at depths of around 10–20 km suggest that the layer may include fluid, clay minerals, and/or serpentine–chlorite (Mochizuki et al., 2005). Stripe-like heterogeneities have been revealed by measurements of this type in the subducting Pacific slab: relatively low-velocity zones correspond to low-seismicity areas in this slab (Nakamura et al., 2008). A region with a high Poisson's ratio may also correspond to a serpentinized mantle wedge and appears to be coincident with the aseismic slip zones, such as the slow-slip and afterslip events (Tahara et al., 2008). Finally and at another scale, one could point out the anomalously low compressional (V_p) and shear (V_s) wave velocities and resistivity within the two creeping zone in the SAFOD drill hole (Zoback et al., 2010).

Another indicator of aseismic creep could be the occurrence of microseismicity, which is often associated with permanent creep

Please cite this article as: Gratier, J.-P., et al., Geological control of the partitioning between seismic and aseismic sliding behaviours in active faults: Evidence from the Western Alps, France, Tectonophysics (2013), http://dx.doi.org/10.1016/j.tecto.2013.02.013

processes, for example along the San Andreas Fault (Nadeau et al., 2004) or in the subduction zone of eastern Japan where repeating slip patches of small asperities of 0.1 to 1 km in size are recorded, these patches being surrounded by stable sliding areas along the plate interface (Uchida et al., 2012). Systematic investigation of the geometry of the creeping and non-creeping zones coupled with a better understanding of the creep mechanism are therefore required in order to predict the variation in strain-rate and stress with time and better understand earthquake nucleation and propagation and related aseismic phenomena along subduction zones.

To model the part accommodated by the creeping behaviour at depth versus the seismic part, both the creep mechanism and the geometry of the creeping zone at depth must be evaluated. The former was one of the aims of this study. The possible geometry of seismic and aseismic zones in subduction zones is given in an imaginative schematic view (Fig. 12) freely drawn from the example of the Nankin area (Tobin et al., 2009). One can distinguish various schematic behaviours:

– some rigid segment are not likely to creep by pressure solution: monomineralic rock, large grain size, low porosity rocks (white in Fig. 12). According to the preceding discussion, such rocks could be low porosity massive sandstone, limestone, or volcanic rocks (with likely high P-wave velocity).

– some weak segments are likely to creep by low friction processes or pressure solution creep and could accommodate the imposed displacement rate with only minor earthquakes (microseismicity): polymineralic rock with small grain size (black in Fig. 12). According to the preceding discussion, such rocks could be fine-grained mixed clay and siltstones, or mixed clay and carbonates (marls) or oceanic sediments with mixing of clay and fine grained oceanic crust minerals (with likely low P-wave velocity).

– finally, some segments are creeping but they could only accommodate part of the imposed rate of deformation, so these segments are likely to show both earthquakes and postseismic creep processes. According to the preceding discussion such rocks have intermediary composition and structure between the two preceding types of rocks.

From a general point of view in this Fig. 12, the rocks with lighter shades are less prone to creep while the ones with darker shades are more prone to creep. In such a context, earthquakes are likely to initiate within the zones where creep is difficult and at the boundary between the creeping and non-creeping zones, their magnitude being proportional to the slip deficit and locked area with possible dynamic propagation through creep zones. The same heterogeneous distribution may be seen in a map view (Zhao et al., 2011), where the main shocks initiate in high P-wave velocity zones, whereas the low velocity zones are more likely to creep. We briefly investigate above which criteria could be used to identify such geometry. This geometry could be investigated by elastic wave velocity measurements at depth. These creeping rocks (fine grained mixed clay and siltstones, or marls) are known to be less rigid than the material likely not to creep (so to break) as low porosity massive limestone, sandstone or volcanic rocks (Bourbie et al., 1987). Another specificity is that pressure solution requires fluids and the presence of such fluid phases could be evidenced at depth. To this end, a classical parameter investigated is the V_p/V_s ratio, which depends on the Poisson's coefficient of the rock. Accordingly, this parameter depends on the nature of the minerals in the rock, but also on its microstructure and fluid content: it increases with fluid content; and it decreases with the existence (or development) of a flat crack network (Brantut et al., 2012).

6. Conclusion

From the studied example of strike-slip and normal faults in the western Alps, it is shown that the transition between seismic and aseismic behaviours is controlled by the geological characteristics of the deformed rocks: limestones are more prone to seismic failure and marls are more prone to aseismic creep along the same fault zone. The reason is that polymineralic marl rocks can creep faster by pressure solution compared to monomineralic limestone. The same concept also applies to other polymineral rocks (shale) that deform more easily by pressure solution creep than monomineralic rock (low porosity sandstones). The solubility of the minerals in solution is a key parameter of the pressure solution rate. It is also worth noting that fractured massive limestone or sandstone are more prone to creep than intact limestone or sandstone thanks to the diffusion short-cut effect of the fracture network; however, this effect lasts only for a limited period due to the progressive sealing of the fractures (post-seismic effect).

Given that creep relaxes at least part of the stress that builds up as a result of the imposed tectonic loading, aseismic patches are likely to act as barriers to earthquake propagation. However, examples are shown of creeping zones that are traversed by earthquakes. This occurs if the creeping process is not efficient enough to lower the stress level or if dynamic ruptures can overpass the creeping zone barrier. Identification of the creep mechanism is thus of crucial interest in this case since it can be used to model the creeping segment and to evaluate the time-dependent stress variations.

It is also important to evaluate the location of possible aseismic zones at depth. This could be based on the measurement of physical properties at depth, for example, with elastic wave velocity measurements due to the specificity of the creeping zone: high fluid content and relatively soft material due to the presence of phyllosilicate minerals mixed with soluble minerals as quartz, calcite, feldspars, serpentines….

Acknowledgments

We thank Kyuichi Kanagawa and two anonymous reviewers for their comments that significantly improved the manuscript.

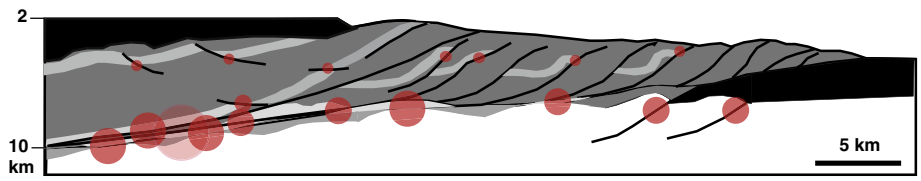

Fig. 12. Schematic view of the possible partition between seismic and aseismic deformations in subduction zones: white segments (with likely high P-Wave velocity) are non-creeping, black segments (with low P-wave velocity) are creeping and accommodate the imposed rate of deformation, grey segments are creeping but accommodate only part of the imposed rate of deformation: the lighter shades are less prone to creep while the darker shades are more prone to creep. Earthquakes (red) are likely to initiate within the lightest zones and at the boundary between the lightest zones. Their magnitude (size of the red circles) is proportional to the slip deficit and locked area with possible dynamic propagation through creep zones (light red). The sketch is freely drawn from the example of the Nankay area (Tobin et al., 2009). The same geologically controlled partition between seismic and aseismic deformations may be seen in map view (Zhao et al., 2011). (For interpretation of the references to color in this figure, the reader is referred to the web version of this article.)

Please cite this article as: Gratier, J.-P., et al., Geological control of the partitioning between seismic and aseismic sliding behaviours in active faults: Evidence from the Western Alps, France, Tectonophysics (2013), http://dx.doi.org/10.1016/j.tecto.2013.02.013

References

Affolter, T., Gratier, J.-P., 2004. Map-view retrodeformation of an arcuate fold-and-thrust belt: the Jura case study. Journal of Geophysical Research 109 (B3), 31–50.

Affolter, T., Faure, J.-L., Gratier, J.-P., Colletta, B., 2008. Kinematic models of deformation at the front of the Alps: new data from map-view restorationx. Swiss Journal of Geosciences 101, 289–303.

Andreani, M., Boullier, A.-M., Gratier, J.-P., 2005. Development of schistosity by dissolution–crystallization in a Californian serpentinite gouge. Journal of Structural Geology 27 (12), 2256–2267.

Andrews, L.M., Railsback, L.B., 1997. Controls on stylolite development: morphologic, lithologic, and temporal evidence from bedding-parallel and transverse stylolites from the US Appalachians. Journal of Geology 105 (1), 59–73.

Arnaud, H., 1975. 1/50,000 Geological map of la Chapelle en Vercors in: S.d.l.c.g.d. France (Editor). Ministère de l'industrie, BRGM, Paris.

Arnaud, H., 1981. De la plateforme urgonienne au basin voconcien: le barremo-bédoulien des Alpes occidentales entre Isère et Buech (Vercors méridional, Diois oriental, Dévoluy), Etat Thesis, University of Grenoble 1, Grenoble.

Arnaud, H., Montjuvent, G., Gonnard, R., 1974. 1/50,000 Geological map of Mens. in: S.d.l.c.g.d. France (Editor). Ministère de l'industrie, BRGM, Paris.

Ashby, M., Verrall, R., 1973. Diffusion-accommodated flow and superplasticity. Acta Metallurgica 21 (2), 149–163.

Bathurst, R.G.C., 1971. Carbonate Sediments and Their Diagenesis. Elsevier, Amsterdam (620 pp.).

Bauerle, G., Bornemann, O., Mauthe, F., Michalzik, D., 2000. Origin of stylolites in Upper Permian Zechstein anhydrite (Gorleben salt dome, Germany). Journal of Sedimentary Research 70 (3), 726–737.

Bjorkum, P.A., Oelkers, E.H., Nadeau, P.H., Walderhaug, O., Murphy, W.M., 1998. Porosity prediction in quartzose sandstones as a function of time, temperature, depth, stylolite frequency, and hydrocarbon saturation. American Association of Petroleum Geologists Bulletin 82 (4), 637–648.

Bjorlykke, K., Hoeg, K., 1997. Effects of burial diagenesis on stresses, compaction and fluid flow in sedimentary basins. Marine and Petroleum Geology 14 (3), 267–276.

Bos, B., Spiers, C.J., 2002. Frictional-viscous flow of phyllosilicate-bearing fault rock: Microphysical model and implications for crustal strength profiles. Journal of Geophysical Research-Solid Earth 107 (B2). http://dx.doi.org/10.1029/2001JB000301.

Bos, B., Peach, C.J., Spiers, C.J., 2000. Frictional-viscous flow of simulated fault gouge caused by the combined effects of phyllosilicates and pressure solution. Tectonophysics 327 (3–4), 173–194.

Bourbie, T., Coussy, O., Zinszner, B., 1987. Acoustic of Porous Media (334 pp.).

Brantut, N., et al., 2012. Dehydration-induced damage and deformation in gypsum and implications for subduction zone processes. Journal of Geophysical Research-Solid Earth 117 (B03205). http://dx.doi.org/10.1029/2011JB008730.

Cara, M., Schlupp, A., Sira, C., 2007. Observations sismologiques: sismicité de la France en 2003, 2004 et 2005. In: Français, B.C.S. (Ed.), ULP/EOST-CNRS/INSU, Strasbourg.

Carrio-Schaffhauser, E., Raynaud, S., Latière, H.J., Mazerolles, F., 1990. Propagation and localization of stylolites in limestones. Geological Society of London, Special Publication 54, 193–199.

Chester, F.M., Chester, J.S., Kronenberg, A.K., Hajash, A., 2007. Subcritical creep compaction of quartz sand at diagenetic conditions: effects of water and grain size. Journal of Geophysical Research-Solid Earth 112 (B06203). http://dx.doi.org/10.1029/2006JB004317.

Chlieh, M., et al., 2011. Interseismic coupling and seismic potential along the Central Andes subduction zone. Journal of Geophysical Research-Solid Earth 116 (B12405). http://dx.doi.org/10.1029/2010JB008166.

Collettini, C., Niemeijer, A., Viti, C., Marone, C., 2009. Fault zone fabric and fault weakness. Nature 462 (7275), 907-U98.

Collettini, C., Niemeijer, A., Viti, C., Smith, S.A.F., Marone, C., 2011. Fault structure, frictional properties and mixed-mode fault slip behavior. Earth and Planetary Science Letters 311 (3–4), 316–327.

Dahlstrom, C.D.A., 1969. Balanced cross section. Canadian Journal of Earth Sciences 6, 743–757.

De Paola, N., et al., 2012. Constraints on Fault Dynamic Weakening Mechanisms from Natural Slip Surfaces in Carbonate Faults. EGU General Assembly Geophysical Research Abstracts, Vienna, Austria, p. 13399.

Demarq, G., Bonnet, A., 1964. 1/50,000 Geological map of Valreas. in: S.d.l.c.g.d. France (Editor). Ministère de l'industrie, BRGM, Paris.

Deville, E., Chauvière, A., 2000. Thrust tectonics at the front of the western Alps: constraints provided by the processing of seismic reflection data along the Chambery transect. Comptes Rendus de l'Academie des Sciences – Series IIA – Earth and Planetary Science 331 (11), 725–732.

Dewers, T., Ortoleva, P., 1990. A coupled reaction/transport/mechanical model for intergranular pressure solution stylolites, and differential compaction and cementation in clean sandstones. Geochimica et Cosmochimica Acta 54, 1609–1625.

Dezes, P., Schmidt, S.M., Ziegler, P.A., 2004. Evolution of the European cenozoic rift system: interaction of the Alpine and Pyrenean orogens with their foreland lithosphere. Tectonophysics 389, 1–33.

Donze, P., Enay, R., 1972. 1/50,000 Geological map of Seyssel. in: S.d.l.c.g.d. France (Editor). Ministère de l'industrie, BRGM, Paris.

Elliott, D., 1983. The construction of balanced cross sections. Journal of Structural Geology 5 (2), 101.

Evans, E.L., Loveless, J.P., Meade, B.J., 2012. Geodetic constraints on San Francisco Bay Area fault slip rates and potential seismogenic asperities on the partially creeping Hayward fault. Journal of Geophysical Research-Solid Earth 117 (B03410). http://dx.doi.org/10.1029/2011JB008398.

Faulkner, D.R., Lewis, A.C., Rutter, E.H., 2003. On the internal structure and mechanics of large strike-slip fault zones: field observations of the Carboneras fault in southeastern Spain. Tectonophysics 367, 235–251.

Flandrin, J. et al., 1975. 1/50,000 Geological map of Nyons. in: S.d.l.c.g.d. France (Editor). Ministère de l'industrie, BRGM, Paris.

Fondriest, M., Smith, S.A., Di Toro, G., Nielsen, S.B., 2012. Mirror-like slip surfaces in dolostone: natural and experimental constraints on a potential seismic marker. In: AGU (Ed.), Fall Meeting, San Francisco, p. S11A-08.

Frayssines, M., Hantz, D., 2009. Modelling and back-analysing failures in steep limestone cliffs. International Journal of Rock Mechanics and Mining Sciences 46 (7), 1115–1123.

Freed, A.M., 2007. Afterslip (and only afterslip) following the 2004 Parkfield, California, earthquake. Geophysical Research Letters 34 (L06312). http://dx.doi.org/10.1029/2006GL029155.

Gratier, J.-P., 2011. Fault permeability and strength evolution related to fracturing and healing episodic processes (years to millennia): the role of pressure solution. Oil & Gas Science and Technology 3, 491–506.

Gratier, J.-P., Ménard, G., Arpin, R., 1989. Strain–displacement compatibility and restoration of the Chaînes Subalpines of the western Alps. Geological Society Special Publication 45, 65–81.

Gratier, J.-P., Guiguet, R., Renard, F., Jenatton, L., Bernard, D., 2009. A pressure solution creep law for quartz from indentation experiments. Journal of Geophysical Research-Solid Earth 114 (B03403). http://dx.doi.org/10.1029/2008JB005652.

Gratier, J.-P., et al., 2011. Aseismic sliding of active faults by pressure solution creep: evidence from the San Andreas Fault Observatory at depth. Geology 39 (12), 1131–1134.

Gratier, J.-P., Dysthe, D.K., Renard, F., 2013. The role of pressure solution creep in the ductility of the Earth's upper crust. Advances in Geophysics 54, 47–179. http://dx.doi.org/10.1016/B978-0-12-380940-7.00002-0.

Gunzburger, Y., Cornet, F.H., 2007. Rheological characterization of a sedimentary formation from a stress profile inversion. Geophysical Journal International 168, 402–418.

Hadizadeh, J., et al., 2012. A microstructural study of fault rocks from the SAFOD: implication for the deformation mechanisms and strength of the creeping segment of the San Andreas Faults. Journal of Structural Geology 42, 246–260. http://dx.doi.org/10.1016/j.jsg.2012.04.011.

Heald, M.T., 1955. Stylolites in sandstones. Journal of Geology 63, 101–114.

Heap, M.J., Baud, P., Meredith, G., Bell, A.F., Main, I.G., 2009. Time dependent brittle creep in Darley Dale sandstone. Journal of Geophysical Research-Solid Earth 114 (B07203). http://dx.doi.org/10.1029/2008JB006212.

Hickman, S.H., Evans, B., 1991. Experimental pressure solution in halite: the effect of grain/interphase boundary structure. Journal of the Geological Society of London 148, 549–560.

Hindle, D., Burkhard, M., 1999. Strain, displacement and rotation associated with the formation of curvature in fold belts; the example of the Jura arc. Journal of Structural Geology 21 (8–9), 1089–1101.

Hoang-Trong, P., Cara, M., 1998. Observations sismologiques: sismicité de la France en 1993–1994–1995–1996. In: Français, B.C.S. (Ed.), ULP/IPGS-INSU, Strasbourg.

Holdsworth, R.E., et al., 2011. Fault rocks from the SAFOD core samples: implications for weakening at shallow depths along the San Andreas Fault, California. Journal of Structural Geology 33 (2), 132–144.

Hossack, J.R., 1979. Use of balanced cross-section in the calculation of orogenic contraction — review. Journal of the Geological Society 136 (11), 705–711.

Ide, S., Baltay, A., Beroza, C., 2011. Shallow dynamic overshot and energetic deep rupture in the 2011 Mw 9.0 Tohoku-oki earthquake. Science 322, 1426–1429.

Ikari, M.J., Niemeijer, A., Marone, C., 2011. The role of fault zone fabric and lithification state on frictional strength, constitutive behavior, and deformation structures. Journal of Geophysical Research-Solid Earth 116 (B08404). http://dx.doi.org/10:1029/2011JB008264.

Jefferies, S.P., et al., 2006. Origin and mechanical significance of foliated cataclastic rocks in the cores of crustal-scale faults: examples from the Median Tectonic Line, Japan. Journal of Geophysical Research-Solid Earth 111 (B12303). http://dx.doi.org/10.1029/2005JB004205.

Lay, T., et al., 2012. Depth-varying rupture properties of subduction zone megathrust faults. Journal of Geophysical Research-Solid Earth 117 (B04311). http://dx.doi.org/10.1029/2011JB009133.

Lehner, F.K., 1995. A model for intergranular pressure solution in open systems. Tectonophysics 245, 153–170.

Lemoine, M., et al., 1986. The continental margin of the mesozoic Tethys in the Western Alps. Marine and Petroleum Geology 3 (3), 179–199.

Lockner, D.A., Morrow, C., Moore, D., Hickman, S., 2011. Low strength of deep San Andreas fault gouge from SAFOD core. Nature 472 (7341), 82-U107.

MacGarr, A., 1988. On the state of lithospheric stress in the absence of applied tectonic forces. Journal of Geophysical Research-Solid Earth 93 (11), 13,609–13,617.

Marone, C., 1998. Laboratory-derived friction laws and their application to seismic faulting. Annual Review of Earth and Planetary Sciences 26, 643–696.

Masson, F., et al., 2005. Seismic versus aseismic deformation in Iran inferred from earthquakes and geodetic data. Geophysical Journal International 160 (1), 217–226.

Mazzotti, S., Leonard, L.J., Cassidy, J.F., Rogers, G.C., Halchuk, S., 2011. Seismic hazard in western Canada from GPS strain rates versus earthquake catalog. Journal of Geophysical Research-Solid Earth 116 (B12310). http://dx.doi.org/10.1029/2011JB008213.

Ménard, G., Thouvenot, F., 1987. Coupes équilibrées crustales: méthodologie et application aux Alpes occidentales. Geodinamica Acta 1 (1), 35–45.

Mittempergher, S., et al., 2011. Evidence of transient increases of fluid pressure in SAFOD phase III cores. Geophysical Research Letters 38 (L0330). http://dx.doi.org/10.1029/2010GL046129.

Please cite this article as: Gratier, J.-P., et al., Geological control of the partitioning between seismic and aseismic sliding behaviours in active faults: Evidence from the Western Alps, France, Tectonophysics (2013), http://dx.doi.org/10.1016/j.tecto.2013.02.013

Mochizuki, K., et al., 2005. Intense PP reflection beneath the aseismic forearc slope of the Japan Trench subduction zone and its implication of aseismic slip subduction. Journal of Geophysical Research-Solid Earth 110 (B01302). http://dx.doi.org/10.1029/2003JB002892.
Molliex, S., Fabbri, O., Bichet, V., Madritsch, H., 2011. Possible Quaternary growth of a hidden anticline at the front of the Jura fold-and-thrust belt: geomorphological constraints from the Foret de Chaux area, France. Bulletin de la Société Géologique de France 182 (4), 337–346.
Nadeau, R.M., Michelini, A., Uhrhammer, R.A., Dolenc, D., McEvilly, T.V., 2004. Detailed kinematics, structure and recurrence of micro-seismicity in the SAFOD target region. Geophysical Research Letters 31 (L12S08). http://dx.doi.org/10.1029/2003GL019409.
Nakamura, M., et al., 2008. Three-dimensional P- and S-wave velocity structures beneath Japan. Physics of the Earth and Planetary Interiors 168 (1–2), 49–70.
Niemeijer, A., Spiers, C.-J., 2005. Influence of phyllosilicates on fault strength in the brittle–ductile transition: insight from rock analogue experiments. Geological Society of London, Special Publication 245, 303–327.
Paterson, M.S., 1973. Nonhydrostatic thermodynamics and its geologic applications. Reviews of Geophysics and Space Physics 11, 355–389.
Perfettini, H., et al., 2010. Seismic and aseismic slip on the Central Peru megathrust. Nature 465 (7294), 78–81.
Raj, R., 1982. Creep in polycrystalline aggregates by matter transport through a liquid phase. Journal of Geophysical Research-Solid Earth 87, 4731–4739.
Ramsay, J.G., 1967. Folding and fracturing of rocks. International Series in the Earth and Planetary Sciences.McGraw-Hill Book Company (568 pp.).
Riedel, W., 1929. Zur Mechanik geologischer Brucherscheinungen. Zentralblatt für Mineralogie, Geologie und Paläontologie 354–368.
Rutter, E.H., 1976. The kinetics of rock deformation by pressure solution. Philosophical Transactions of the Royal Society of London 283, 203–219.
Saffer, D.M., Marone, C., 2003. Comparison of smectite- and illite-rich gouge frictional properties: application to the updip limit of the seismogenic zone along subduction megathrusts. Earth and Planetary Science Letters 215, 219–235.
Satyabala, S.P., Yang, Z.H., Bilham, R., 2012. Stick-slip advance of the Kohat Plateau in Pakistan. Nature Geoscience 5 (2), 147–150.
Schleicher, A.M., Tourscher, S.N., van der Pluijm, B.A., Warr, L.N., 2009. Constraints on mineralization, fluid–rock interaction, and mass transfer during faulting at 2–3 km depth from the SAFOD drill hole. Journal of Geophysical Research-Solid Earth 114. http://dx.doi.org/10.1029/2008JB006092.
Scholz, C., 1998. Earthquakes and friction laws. Nature 391, 37–42.
Smith, B.J., Holdsworth, R.E., Collettini, C., Pearce, M.A., 2012. The microstructural character and mechanical significance of fault rocks associated with a continental low-angle normal fault: the Zuccale Fault, Elba Island, Italy. Geological Society of London, Special Publication 359, 97–113.
Tahara, M., et al., 2008. Seismic velocity structure around the Hyuganada region, Southwest Japan, derived from seismic tomography using land and OBS data and its implications for interplate coupling and vertical crustal uplift. Physics of the Earth and Planetary Interiors 167 (1–2), 19–33.
Thibaut, M., Gratier, J.-P., Léger, M., Morvan, J.-M., 1996. An inverse method for determining three dimensional fault geometry with thread criterion: application to strike-slip and thrust faults (Western Alps and California). Journal of Structural Geology 18, 1127–1138.
Thomas, A.R., Dahl, W.M., Hall, C.M., York, D., 1993. 40Ar/39Ar analyzes of authigenic muscovite, timing of stylolitization, and implications for pressure solution mechanisms: Jurassic Norphlet formation, offshore Alabama. Clays and Clay Minerals 41 (3), 269–279.
Thouvenot, F., et al., 1998. The M-L 5.3 Epagny (French Alps) earthquake of 1996 July 15: a long-awaited event on the Vuache Fault. Geophysical Journal International 135 (3), 876–892.
Thouvenot, F., Fréchet, J., Jenatton, L., Gamond, J.-F., 2003. The Belledonne Border Fault: identification of an active seismic strike-slip fault in the western Alps. Geophysical Journal International 155 (1), 174–192.
Thouvenot, F., Jenatton, L., Gratier, J.-P., 2009. 200-m-deep earthquake swarm in Tricastin (lower Rhone Valley, France) accounts for noisy seismicity over past centuries. Terra Nova 21 (3), 203–210.
Tobin, H., et al., 2009. NantroSEIZE Stage1 Expeditions: Introduction and Synthesis of Key Results. Proceeding IODP. http://dx.doi.org/10.2204/iodp.proc.314315316.101.2009.
Tourette, A., 2008. Caractérisation de la déformation ductile et fragile sur la faille de la Cléry (Vercors) Bachelor's degree, University of Grenoble 1, Grenoble, 11 pp.
Uchida, N., et al., 2012. Source parameters of microearthquakes on an interplate asperity off Kamaishi, NE Japan over two earthquake cycles. Geophysical Journal International 189 (2), 999–1014.
van Noort, R., Spiers, C., Peach, C., 2007. Effects of orientation on the diffusive properties of fluid-filled grain boundaries during pressure solution. Physics and Chemistry of Minerals 34 (2), 95–112.
Verberne, B.A., He, C., Spiers, C.J., 2010. Frictional properties of sedimentary rocks and natural fault gouge from the Longmen Shan Fault zone, Sichuan, China. Bulletin of the Seismological Society of America 100 (5B), 2767–2790.
Wangen, M., 1998. Modeling porosity evolution and cementation of sandstones. Marine and Petroleum Geology 15 (5), 453–465.
Weibel, R., Keulen, N., 2008. Diagenesis influencing the porosity of Upper Jurassic reservoir sandstones, Danish North Sea. Geological Survey of Denmark and Greenland Bulletin 15, 9–12.
Weyl, P.K., 1959. Pressure solution and the force of crystallization: a phenomenological theory. Journal of Geophysical Research-Solid Earth 64, 2001–2025.
Wibberley, C.A.J., Shimamoto, T., 2005. Earthquake slip weakening and asperities explained by thermal pressurization. Nature 436. http://dx.doi.org/10.1038/nature03901.
Wicks, C., et al., 2011. InSAR observations of aseismic slip associated with an earthquake swarm in the Columbia River flood basalts. Journal of Geophysical Research-Solid Earth 116 (B12304). http://dx.doi.org/10.1029/2011JB008433.
Ye, L.L., Lay, T., Kanamori, H., 2012. The Sanriku-Oki low-seismicity region on the northern margin of the great 2011 Tohoku-Oki earthquake rupture. Journal of Geophysical Research-Solid Earth 117 (B02305). http://dx.doi.org/10.1029/2011JB008847.
Zhang, X.M., Spiers, C.J., Peach, C.J., 2010. Compaction creep of wet granular calcite by pressure solution at 28 degrees C to 150 degrees C. Journal of Geophysical Research-Solid Earth 115. http://dx.doi.org/10.1029/2008JB005853.
Zhao, D., Huang, Z., Umino, N., Hasegawa, A., Kanamori, H., 2011. Structural heterogeneity in the megathrust zone and mechanism of the 2011 Tohoku-oki earthquake (Mw 9.0). Geophysical Research Letters 38 (L17308). http://dx.doi.org/10.1029/2011gl048408.
Zoback, M., Hickman, S., Ellsworth, W., 2010. Scientific drilling into the San Andreas Fault Zone. EOS. Transactions of the American Geophysical Union 91 (22), 197–199.
Zubtsov, S., et al., 2004. Experimental pressure solution compaction of synthetic halite/calcite aggregates. Tectonophysics 385 (1–4), 45–57.

Please cite this article as: Gratier, J.-P., et al., Geological control of the partitioning between seismic and aseismic sliding behaviours in active faults: Evidence from the Western Alps, France, Tectonophysics (2013), http://dx.doi.org/10.1016/j.tecto.2013.02.013